MSc Mechanical Engineering

Running Free: Wireless sEMG Garment for Tracking Runner's Muscle Fatigue

Koen Jongbloed

TU Delft

Running Free: Wireless EMG Garment for Tracking Runner's Muscle Fatigue

Koen Jongbloed

in partial fulfilment of the requirements for the degree of

Master of Science
in Mechanical Engineering

at Delft University of Technology,
to be defended publicly on Thursday November 23, 2023 at 9:00 AM.

Supervisor:	Dr. ir. E. van der Kruk	TU Delft
	Dr. R. J. de Vos	Erasmus MC
Thesis committee:	Dr. ir. E. van der Kruk	TU Delft
	Dr. R. J. de Vos	Erasmus MC
	Prof. dr. F.C.T. van der Helm	TU Delft

TU Delft Delft University of Technology

CONTENTS

Running Free: Wireless EMG Garment for Tracking Runner's Muscle Fatigue

TU Delft - November 15, 2023
K.J.P. Jongbloed (4381572)
Supervisors:
Dr. ir. E. van der Kruk
Dr. R. J. de Vos

Abstract— Muscle fatigue's indirect link to higher athletic injury risks is a key focus of this study. It highlights how fatigue-induced shifts in muscle resource allocation and movement patterns can lead to biomechanical imbalances, subsequently heightening injury susceptibility. Addressing high injury rates in athletics, this study was conducted in two pivotal phases: the development of a wearable, textile-integrated surface electromyography (sEMG) garment, and the identification of the most effective real-time fatigue metric for true wireless detection for dynamic exercise. While traditional sEMG methods provide valuable insights in laboratory settings, they fall short in dynamically and individually monitoring muscle fatigue in real-world scenarios.

The initial phase focused on creating a smart garment with integrated textile-based electrodes named the RunWave. The second phase concentrated on analyzing muscle fatigue during dynamic running activities, employing an incremental treadmill exercise test. Fatigue was assessed using cardiorespiratory metrics and Borg's Rate of Perceived Exertion (RPE), alongside the evaluation of six fatigue metrics: Average Rectified Value (ARV), approximate and sample entropy, instantaneous mean and median frequencies, and Dimitrov's Spectral Fatigue Index. Significant differences between fatigued and non-fatigued states were observed, especially noted in shifts in entropy, mean and median frequencies, and most prominently in ARV. These findings underscored the necessity for personalized fatigue monitoring strategies, given the variation in fatigue onset and subjective exhaustion experiences among individuals.

The RunWave, with its focus on the ARV metric, emerged as particularly promising for fatigue detection. ARV's computational simplicity and interpretability make it ideal for real-world applications. Despite initial challenges such as fitment issues, electronic limitations, and garment robustness, the RunWave garment was positively received for its comfort and practicality. With targeted improvements, the RunWave garment, leveraging ARV, shows great potential for effectively monitoring muscle fatigue in runners, suggesting a substantial step forward in reducing injury risks in athletic contexts.

1. Introduction

Fatigue is a complex phenomenon that greatly affects athletes' performance and health. It generally refers to any reduction in performance caused by physical or mental factors, or a combination of both [1]. Particularly in competitive sports, such as soccer, muscle injuries, often linked to fatigue, account for a significant proportion of time lost in training and competition [2]. This underscores the critical need for effective fatigue monitoring, not just for enhancing performance but also for reducing injury risks.

However, the landscape of fatigue monitoring is predominantly lab-centric, with a vast majority of studies conducted under controlled laboratory conditions (81.7% [3]). Field studies typically depend on tools like Inertial Measurement Units (IMUs) and Heart Rate (HR) sensors, which may fall short in providing a holistic understanding of fatigue-related changes. Recent developments in surface electromyography (sEMG) have shed light on muscle activity and fatigue, offering a variety of analytical methods. This includes metrics such as the Average Rectified Value (ARV) [4], time-frequency measures like instantaneous mean and median frequencies [5], spectral fatigue indices like Dimitrov's FInsm5 [6], and analyses of complexity using entropy metrics [7].

Despite the insights offered by these methods, their application has largely been confined to lab settings, with a focus on static or controlled dynamic movements. Their interaction and the temporal dynamics of fatigue onset and progression during highly dynamic activities such as running remain underexplored. Furthermore, there is a growing need for advanced, field-applicable fatigue monitoring systems that can unobtrusively track a broad spectrum of physiological and psychological markers.

The aim of this study is twofold: to develop a practical and wearable smart garment, named the RunWave, for in-field fatigue monitoring using textile-based surface electromyography, and to determine the most suitable fatigue metric for use with this garment. By addressing these objectives, the study seeks to bridge the gap between laboratory research and real-world applications, enhancing our understanding and capability to monitor fatigue effectively in dynamic sports environments.

2. Methods

In summary, we developed an instrumented smart garment (the RunWave) designed for wireless surface electromyography (sEMG) data collection to investigate running-induced local muscle fatigue. This section delves into the various aspects of the study's methodology, starting with an overview of the specially designed RunWave garment. It then proceeds to discuss the experimental design and participant selection criteria, providing the rationale behind the chosen protocols. Subsequent sections outline the data pre-processing techniques employed, setting the stage for later analyses. Metrics for quantifying muscle fatigue are elaborated upon, as are the methods for validating both the experimental setup and these metrics. All methods and data analyses were carried out us-

ing Python programming language v3.11.4 (Python Software Foundation) [8].

2.1. RunWave Design

In the realm of dynamic sports like running, where the study of muscle fatigue is crucial, existing sEMG systems often fall short in real-world applicability. A primary limitation is the compromise between what is termed 'true wireless' functionality and system portability. For the purposes of this study, 'true wireless' is defined as a system's ability to operate autonomously, free from any physical or wireless attachments to a host device. An additional limitation lies in the necessity for professional involvement in system setup and data collection. Current sEMG systems typically require professionals not only to attach the device but also to ensure its proper functioning, thereby restricting the feasibility of longitudinal studies in real-world, dynamic settings.

While existing wireless sEMG systems may boast a wide range of functionalities, such as EEG and HD-sEMG capabilities, these come at the expense of device size and obtrusiveness (TMSI, SAGA 32/64/128). Most of these systems are designed with wireless capabilities in mind, rather than being optimized for unobtrusive use or active sports settings. As a result, they are typically bulky and impractical for localized muscle fatigue detection in scenarios that require free movement.

The RunWave is designed to address these limitations through the following key requirements:

True Wireless Surface Electromyography

- No wires to external systems for both data acquisition and power.
- Local data storage, with the option for wireless transmission, to ensure no range limits to the receiver.

Portable and Unobtrusive system

- Low weight and small size to minimize impact on the movement.
- Design features to minimize interference with desired movement patterns, ensuring the garment stays securely in place.

Realistic Measurement Conditions

- In-field: Moving the measurements from a controlled laboratory setting to in-field measurements.
- User-friendly design: The RunWave is designed for effortless operation, even by non-professionals. The RunWave is easily aligned using two boney landmarks: the vertical line on the elastic band has to be aligned with the tibia and the top band should be just below the tuberosity of the tibia.
- Skin-Friendly Electrodes: Minimize data loss due to sensor detachment and improving user comfort.
- Self-Contained Operation: All data is locally stored and no required external synchronization with a base station.
- Compatibility with Everyday Wear: Designed to be compatible with regular-height socks and shin guards, the RunWave ensures both comfort and data accuracy during use.

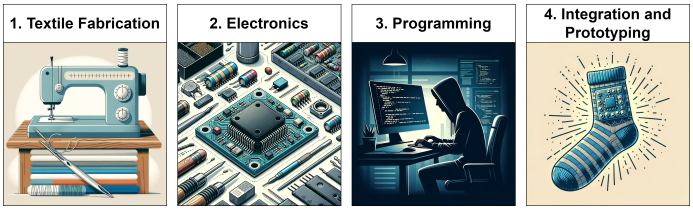

Fig. 1: Stages of RunWave Design and Development. (1) Textile Fabrication illustrating the crafting of the device's fabric; (2) Electronics detailing the hardware components used; (3) Programming showcasing the software and coding aspect; and (4) Integration and Prototyping representing the culmination of all elements into a functional prototype.

Figure 1 presents the four crucial stages of the RunWave garment's evolution, from its inception to its ultimate form. In the subsequent subsections, we'll delve deeper into each stage, elucidating the design choices and hurdles overcome to tailor the garment for endurance sports efficacy.

2.1.1. Textile Fabrication: The RunWave's foundation consists of a thick elastic band, flanked by three narrower elastic bands on the outer sides and in the middlel (Figure 2b). These narrower bands feature a silicone coating to keep the garment in place during exercise. The device is closed using eye-hook fasteners located at the short ends of the main band (Figure 2a). The electrodes are fabricated from silver-coated neoprene and function as dry-contact electrodes [9](Figure 2c and 2d). Due to the higher skin-electrode resistance and variability in textile-based electrodes compared to standard silver electrodes [10] [11], the contact surface area has been expanded from $1cm^2$ to $4.5cm^2$ [12]. The inter-electrode distance (IED) follows the SENIAM guidelines at 20mm [12]. Electrode-skin pressure is achieved through the natural thickness of the neoprene material and the radial tension from the fastened bands [11]. When the electrodes are connected to the microcontroller system, shielded conductive yarn is used, which is secured with specialized sewing techniques to minimize yarn stretch [10]. This approach is implemented to reduce variations in resistance, a common issue when conductive yarn changes length, such as during stretching. This alteration in resistance due to yarn elongation can lead to fluctuating electrical properties.

2.1.2. Electronic system design: The data acquisition system centres around an ESP32 system-on-chip (SoC) microcontroller unit (MCU), seen in Figure3b. It features BLE, WiFi, and a 12-bit Analog-to-Digital Converter (ADC) [13]. Given the ADC's 12-bit resolution, additional hardware filtering and signal amplification are required, achieved through a custom four-stage circuit, seen in Figure 3a. Detailed schematics and associated calculations of this circuit are comprehensively provided in the Appendix, specifically in Figures 6 and 7, for reference throughout this discussion.

The initial stage employs an instrumentation amplifier to negate the need for impedance matching between the input

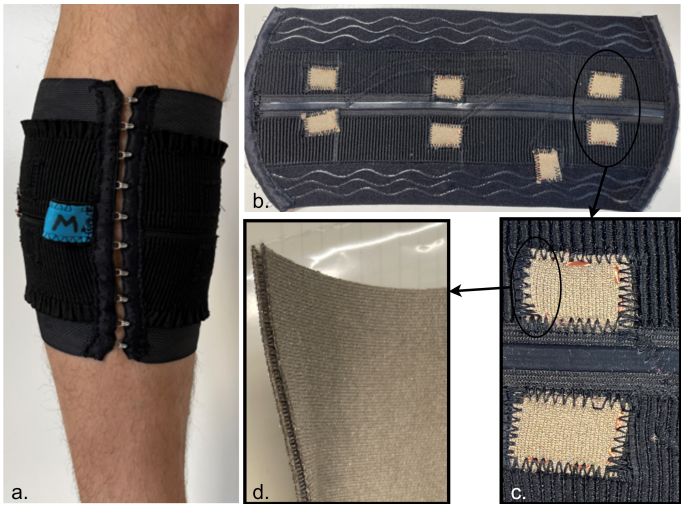

Fig. 2: Overview of Textile Fabrication. (a) hook-fasteners; (b) central elastic band connected to three smaller bands with silicone coating and three sets of bipolar electrode pairs; (c) bipolar electrode pair; (d) silver coated neoprene material.

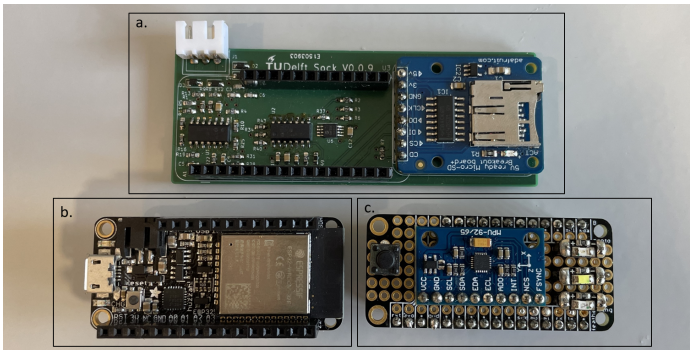

Fig. 3: Electronic System Design. (a) Custom four-stage amplification and filtering PCB; (b) ESP32 SoC Featherboard by Adafruit; (c) Auxiliary PCB with LEDs, MPU6500, and button.

electrodes, a critical feature given the varying impedance of textile electrodes [14]. Its high input impedance and common-mode rejection ratio (CMRR of 103) make it well-suited for capturing bio-physiological signals [15]. The gain resistor of the instrumentation amplifier is chosen such that the gain is relatively low ($G_{inst} = 10.81$). This helps ensure that high power noise does not saturate the input range of the microcontroller, thereby preserving the actual fluctuations of the sEMG signal for accurate measurement.

In the second stage, a Sallen-Key second-order active high-pass filter is implemented, with a cutoff frequency of 18.5 Hz and a gain factor of 2. The decision to use an active filter, as opposed to a passive variant, was predicated on the inherent stability of active filters; notably, their output remains invariant irrespective of load variations. Additionally, active filters provide the capacity to confer supplementary gain to the signal, a significant advantage in the context of this study.

Following this, the third stage includes an inverting amplifier that uses a programmable digital potentiometer (MCP4561-104E/MS), allowing for gain adjustments between 1.34 and 19.20.

The final stage incorporates a Sallen-Key second-order active low-pass filter with a cutoff frequency of 530 Hz and a gain of 7.31. To accommodate these components, a custom PCB has been designed seen in Figure 3a. This board allows the ESP32 MCU to mount directly on top and includes integrated local micro SD storage. An auxiliary PCB, shown in Figure 3c, enhances the system's capabilities by incorporating an MPU6500 sensor for inertial measurements, LED lights for real-time user feedback, and a button for interactive functionalities.

2.1.3. Programming: The system's programming in C and C++ is tailored for high-performance data processing. Analog sampling operates at 1.400 Hz, archiving data onto a microSD card in binary format. This approach minimizes storage overhead, as storing data in ASCII format proved too latency-prone for the system's operational requirements. A dedicated program has been implemented to convert the binary data to ASCII format to facilitate data retrieval and post-processing. This program also accounts for endianness—the order byte sequences are stored in computer memory—to ensure data integrity and facilitate interpretation across different computing environments.

An Interrupt Service Routine (ISR) maintains the high-frequency sampling rate. To further secure data integrity, a dual circular buffer architecture is implemented, acting as a safeguard against premature data overwrites. Utilizing the multi-core capabilities of the microcontroller, measurements of the analog signal are processed and temporarily stored in flash memory on core 0. Core 1 is dedicated to continuously monitoring the state of the full inactive buffer, readying it to be written to the local storage device. A comprehensive feedback and file management system has also been designed to preclude the accidental overwriting of existing data and monitor the consistency of the sampling frequency over time.

2.1.4. Prototyping and Integration: The data acquisition system is securely housed within a custom-designed 3D-printed enclosure, featuring integrated loops for fastening the system to the lower leg at a location distal to the medial tibial plateau as shown in Figure 4. This strategic positioning minimizes system movement during physical activity. Electrical connectivity between the conductive yarn and the MPU is ensured through a durable 3-pin JST connector. To bolster stability, the electronic enclosure employs a double-sided tape Velcro system. One adhesive side of the Velcro is secured to the housing, while the counterpart is fixed to the designated area on the textile garment, reducing potential oscillations. Complementing this, a high-elastic band featuring a silicone coating wraps around the leg to further optimize the device's securement. The system derives its power from a separately attached lithium-ion battery.

2.2. Experimental design and protocol

The principal objective of this study is to assess the ability of various surface electromyography (sEMG) metrics to identify the onset and progression of local muscle fatigue

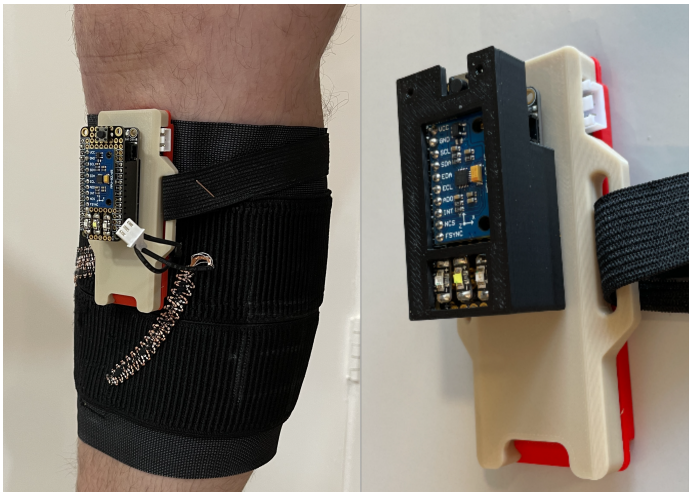

Fig. 4: RunWave Garment with Custom FDM Encasing. This image displays the garment with integrated textile electrodes and electronics housed in a durable, FDM encasing for securing to the leg and physical protection.

during running-based activities. While the ultimate aim is to implement these metrics in wearable technology for in-field monitoring, this research specifically focuses on evaluating which metric is most reliable and suitable for detecting fatigue onset and progression.

2.2.1. Participant selection: In our study, we enlisted a group of 5 healthy male adults, ranging in age from 24 to 30. All participants were required to be devoid of any injuries (see Appendix E Table XII). The term ”healthy” specifies that participants must have no respiratory or cardiovascular conditions, or any other medical issues, that could interfere with the execution of the exercise test. Likewise, the term ”injury” refers to any condition—acute or chronic—that could influence the participant's natural movement patterns. This includes acute musculoskeletal issues like sprains affecting muscles, tendons, or ligaments, as well as any long-lasting limitations due to past injuries. All participants are recreationally active individuals, although they are not necessarily regular runners. While they have some experience with running, it is not a consistent part of their regular physical activity routine.

2.2.2. Experimental protocol: Each participant is equipped with a portable metabolic device (Cosmed, K5) and six sEMG sensors (Trigno Avanti, Delsys). The sensors are positioned bilaterally on the gastrocnemius lateralis, medialis and the tibialis anterior muscles. The placement of these sensors adheres to the SENIAM (Surface ElectroMyoGraphy for the Non-Invasive Assessment of Muscles) guidelines to ensure methodological rigour and reliability in the sEMG readings [12]. The treadmill test begins with a 6-minute walking session at 4 km/h. This initial phase serves multiple purposes: it allows the participants to acclimate to the equipment, collect baseline measurements for later comparison, and offer a gentle warm-up to the subsequent test phases.

Following this preparatory phase, the treadmill speed is 6 km/h. At this juncture, the speed is incremented every minute while participants' rate of perceived exertion (RPE) was continually assessed. A suite of hand signals facilitates real-time RPE communication: a closed fist signifies no perceptual change, a thumbs-up indicates an increase in exertion, and a horizontal hand oscillating from side to side signals an RPE of 13 or ”somewhat hard.” The treadmill velocity was fixed when a participant conveys this ”somewhat hard” status. The session persists at this plateau until the participant reaches an RPE of 17 or 18, denoted as ”very hard,” at which juncture they are empowered to halt the treadmill session autonomously.

The rationale for adopting this protocol, referred to as the standard induced fatigue protocol (RIF), stems from its ability to accommodate subjective variation in participants' fitness levels and perceived exertion. This negates the need for personalized protocols that would otherwise require pre-existing performance data or preliminary tests to establish appropriate settings, as cited in Koen Jongbloed (2022) [3].

2.3. Data Pre-Processing

2.3.1. Surface EMG data: Sensors corresponding to the same participant, being synchronized, are anticipated to possess nearly identical, if not entirely identical, counts of sampled data points. If a sensor ceased measuring prematurely, it would still exhibit the same number of data entries. However, its timestamps would be represented as NaN values and all corresponding data values set to zero. Any sensor presenting a column populated with such NaN timestamps and paired with zero data values was identified as malfunctioning and subsequently excluded from further analysis.

Data sets with more than 20% missing data were disregarded for further study. Additionally, visual inspection of amplitude versus time plots was carried out to identify any instances of sensor detachment, which would be evident from a saturated signal or completely flat lining. Any data set showing such behavior was excluded.

The original data, sampled at 1259Hz, were resampled to 800Hz to improve computational efficiency. The resampled data was filtered with a fourth-order Butterworth bandpass filter with cut-of frequencies of 15Hz and 400Hz. Fast Fourier Transform (FFT) analysis was used to identify any extraneous noise originating from power lines and removed using a notch filter at 50Hz including higher order harmonics.

Lastly, one-sample outliers in the semg data sets were identified using the Isolation Forest Outlier detection algorithm (e.g. due to biological interference or electrode movement) . This was done using a contamination factor of 0.0003 and 400 estimators. Detected outliers were subsequently imputed using K-Nearest Neighbors (KNN) imputation (from scikit-learn v1.3.2 module ensable.IsolationForest and impute.KNNImputer).

2.3.2. Cardiorespiratory data: Cardiorespiratory data was assessed on both data quality and reliability for which three physiological features were used for consistency for all participants: the Respiratory Frequency (Rf), Oxygen Consumption (VO2), and Respiratory Exchange Ratio (RER). These features were visually inspected for temporal consistency, validity of temporal development, and alignment with existing literature. Any data that diverged significantly from established norms—potentially indicating system malfunction or improper

mask fitting leading to air leakage—resulted in the exclusion of that particular participant from further analysis.

Additionally, data points exhibiting peaks that exceeded 200% of the amplitude relative to 5 surrounding breath values were treated as outliers and subsequently removed. Zero values were also eliminated from the data set. The presence of high peaks or zero values could arise due to transient issues in the breath-by-breath metabolic system, such as temporary mask displacement, coughing, or irregular breathing patterns, potentially skewing the data.

2.4. Calculation of Metrics

2.4.1. Average Rectified Value: The Average Rectified Value (ARV) is a commonly used estimate in surface electromyography (sEMG) signals analysis [4]. It is an amplitude-based parameter that quantifies the absolute value of the myoelectrical signal, effectively describing the average muscle excitation [16] over a window of time. The ARV is a simple yet effective metric for capturing the overall level of muscle excitation. Because it involves taking the absolute value of the signal, ARV is sensitive to both positive and negative deviations from the baseline, making it an excellent descriptor of signal magnitude regardless of polarity [17]. Its relative robustness also makes it compatible with lower-cost or less precise recording systems, a feature particularly advantageous when considering the potential use of textile-based sEMG electrodes.

Past studies have shown that sEMG amplitude tends to increase during submaximal dynamic exercise and decrease over time during exercises performed at maximal levels of voluntary contraction [18]. These amplitude changes suggest that changes in ARV may serve as a valuable indicator for tracking muscle fatigue, aligning well with this study's objectives.

Mathematically, the ARV of an sEMG signal $x(t)$ over a window of N samples is defined as:

$$\text{ARV} = \frac{1}{N}\sum_{i=1}^{N}|x(i)| \tag{1}$$

In the analysis of the semg data, the ARV was calculated using a sliding window average with a window size of 1200 samples and a step size of 400 samples. This approach was selected to effectively smooth out short-lived fluctuations, thereby enhancing the robustness of the analysis particularly for observing long-term or transient changes. It's important to note that while the sliding window technique mitigates edge effects to a degree, it does not entirely eliminate these distortions, although it offers advantages over a basic window average in this regard.

2.4.2. Instantaneous Mean and Median Frequency: As fatigue sets in, the sEMG signal undergoes a notable frequency shift. Specifically, higher frequency bands, associated with fast-twitch muscle fibers' recruitment and firing rates, tend to decrease [19]. Conversely, lower frequency bands, indicative of the engagement of slow-twitch muscle fibers, often increase. This shift towards lower frequencies and the accompanying decrease in median frequency values are attributable to the reduced number and synchronization of active motor units [20]. These physiological adaptations indicate the body's strategy to maintain muscle performance by increasingly relying on fatigue-resistant slow-twitch fibers [21]. Such shifts in frequency parameters are, therefore, compelling indicators of the onset and progression of muscle fatigue [22]. The frequency shift in time is encapsulated by the instantaneous mean (IMNF) and median frequencies (IMDF), which differ from their traditional counterparts in their ability to provide time-resolved metrics. While the regular mean and median frequencies offer a single value that summarizes the entire signal or larger temporal windows, the instantaneous versions are calculated at multiple time points, offering a dynamic profile that tracks frequency changes over time. This makes the instantaneous metrics more sensitive to transient and local shifts, providing a more nuanced view of muscle fatigue onset and progression.

$$CWT_x(a,b) = \frac{1}{\sqrt{|a|}}\int_{-\infty}^{\infty} x(t)\psi^*\left(\frac{t-b}{a}\right)dt \tag{2}$$

$$\text{IMNF}(t) = \frac{\sum_{i=1}^{N} f_i \cdot |W(f_i,t)|^2}{\sum_{i=1}^{N}|W(f_i,t)|^2} \tag{3}$$

$$\sum_{f_i<f_{\text{med}}}|W(f_i,t)|^2 = \sum_{f_i\geq f_{\text{med}}}|W(f_i,t)|^2 \tag{4}$$

Due to the non-stationary nature of sEMG signals during dynamic contractions in running, traditional Fourier Transform methods are less effective [18]. To better capture temporal shifts in muscle fatigue, this study utilizes Continuous Wavelet Transformation (CWT) [23], as described in Equation 2, to calculate the IMNF and IMDF, described in Equations 3 and 4.

Considering the dynamic and non-stationary characteristics of sEMG signals during running, traditional Fourier Transform methods often fall short in effectiveness [18]. To more accurately capture the temporal variations associated with muscle fatigue, this study employs the Continuous Wavelet Transformation (CWT), a technique better suited for such analysis [23]. The CWT is mathematically detailed in Equation 2. Additionally, to compute the Instantaneous Mean Frequency (IMNF) and Instantaneous Median Frequency (IMDF), we refer to Equations 3 and 4, which provide the necessary formulas for these calculations.

The IMNF and IMDF are not singular values but sequences of mean or median frequencies determined for each time instance [5]. CWT yields a high-dimensional, time-varying profile of these frequencies, effectively capturing the dynamic nature of muscle contractions during the exercise protocol. These sequences offer a granular, 'frame-by-frame' view of muscle activation changes over time.

2.4.3. Dimitrov's Spectral Fatigue Index (FInsm5): While traditional frequency domain analyses, like the Fourier Transform, generally assume signal stationarity, specific approaches are more robust to the non-stationary nature of signals. Herein lies the strength of Dimitrov's Spectral Fatigue Index (FInsm5) [6]. "FInsm5" essentially refers to a Fatigue Index derived using the fifth normalized spectral moment (nsm5). Despite its

operation in the frequency domain, the methodological rigour and specificity of FInsm5 make it a robust metric for such non-stationary signals.

FInsm5 serves as a robust fatigue index that captures the shift in power distribution across the frequency spectrum, effectively weighting different frequency components. As fatigue sets in, the index decreases, reflecting the body's adaptive recruitment of more fatigue-resistant, slow-twitch muscle fibers. This makes FInsm5 a reliable metric for assessing muscle fatigue, particularly in dynamic activities like running where non-stationary signal characteristics are prevalent.

$$\text{FInsm5} = \frac{\int_{f1}^{f2} f^{-1} \cdot PSD(f)\, df}{\int_{f1}^{f2} f^{5} \cdot PSD(f)\, df} \tag{5}$$

FInsm5 is calculated using the power spectral density (PSD) of the sEMG signal within a specific frequency range f_1 to f_2, as described in Equation 5. The formula comprises two integral terms: the numerator focuses on lower frequencies by dividing the PSD by the frequency, while the denominator accentuates higher frequencies by multiplying the PSD with the frequency raised to the fifth power. The choice of exponents -1 and 5 is deliberate, providing a balanced representation of muscle frequencies useful for fatigue analysis.

Due to the reliance of this method on frequency analysis, it does not provide instantaneous results. Consequently, to calculate the index value with greater reliability, the study adopts a strategy of analyzing time windows of 10 seconds, with an step size of 1 second for each subsequent window. Such an extended time frame is essential because shorter segments may not accurately represent the frequency content. The use of 10-second windows is a strategic balance, offering a comprehensive view of the muscle's dynamic response while maintaining temporal resolution for practical analysis.

2.4.4. Approximate and Sample Entropy: Entropy measures the complexity and unpredictability of a system. When a signal becomes more predictable, which corresponds to a lower entropy value, it often indicates a loss of system complexity or adaptability [7]. This reduced entropy may signify an impaired ability of the system to dynamically adjust to changing conditions, possibly highlighting an onset or progression of fatigue [24] [25], system degradation, or loss of functionality.

Both Sample Entropy (SampEn) and Approximate Entropy (ApEn) are employed in this study to quantify the complexity or unpredictability of time-series data.

Sample Entropy is calculated by evaluating the degree of similarity between different subsequences of a given length within the data set, defined in Equation 6. In this evaluation, 'self-matches'—which are instances where a sequence is compared with itself—are not included. This involves counting how often sequences that are similar within a certain tolerance occur, thereby offering a more nuanced view of data complexity. By excluding self-matches, Sample Entropy becomes a robust metric that is less dependent on the length of the data series. As a result, it is generally less sensitive to noise and offers more reliable results for shorter data sequences.

$$\text{SampEn}(m, r, N) = -\ln\left(\frac{A}{B}\right) \tag{6}$$

In Equation 6, A is the number of $(m+1)$ long matching vectors within tolerance r, and B is the number of m-long matching vectors within tolerance r.

Approximate Entropy is computationally more efficient partly because it includes self-matches, simplifying the calculation process by reducing the number of exclusions, defined in Equation 7. However, this feature can make the measure less reliable for noisy or short data sets, as the inclusion of self-matches can artificially lower the entropy value

$$\text{ApEn}(m, r, N) = \phi^{m}(r) - \phi^{m+1}(r) \tag{7}$$

The ApEn and SampEn are calculated using an embedding dimension of $m = 2$ [26], as described in Equations 6 and 7. The threshold or similarity criterion (r) for comparing sequences is derived from the standard deviation (SD) of the time series, specifically set as $r = 0.2 * SD$ [27]. For each entropy calculation, a window of 1200 samples is used, and computations are performed at a step size of 200 samples to slide the window across the data series.

To concentrate on the changes in neuromuscular control that occur during periods of steady-state running and to minimize the impact of the participant's adaptations to velocity shifts, the study's analysis strategy is carefully designed. Given that the experimental protocol involves incremental increases in running velocity, it's essential to select segments of data that most accurately reflect a 'constant' running state. Therefore, for each stage of the experiment, which typically lasts a minute and involves a specific running velocity, only the middle 30 seconds of data are examined. This approach ensures that the analysis focuses on periods where the participant's running velocity is presumed to be stable, providing a more accurate assessment of neuromuscular control during these phases.

2.5. Fatigue Indicators for Fatigue Validation

The validation of fatigue in this study relied on objective cardiorespiratory measures and subjective ratings.

2.5.1. Subjective Fatigue Assessment: Participants' perceived exertion levels were gauged using Borg's Rating of Perceived Exertion (RPE) scale [28], a widely recognized tool for assessing an individual's perception of exercise intensity. This scale, ranging typically from 6 to 20, correlates subjective feelings of exertion with actual physical activity levels. Detailed overview of Borg's RPE scale can be found in Appendix E Table XI. The experimental endpoint in this study was purposefully set to coincide with an RPE score exceeding 17, which falls into the category of 'very hard' on the Borg scale. This level of exertion reflects a high intensity of effort, where participants perceive their physical activity as challenging and demanding.

2.5.2. Objective Fatigue Assessment:

a) Anaerobic Threshold (Ventilatory Threshold 2 - VT2: Determined via the Cosmed K5 system, VT2 was identified when participants reached a RER of 1.0, signaling the onset of anaerobic metabolism—a physiological hallmark of fatigue.

b) Respiratory Exchange Ratio (RER): A RER surpassing 1.10 indicates a significant lactate accumulation and elevated CO_2 production, reflective of anaerobic metabolism [29]. Achieving or exceeding this RER value provides an objective confirmation of metabolic fatigue.

c) Age-Predicted Maximal Heart Rate: Heart rate measurements are often used to assess exercise intensity, aerobic and anaerobic thresholds, and to determine training zones. Participants were evaluated based on whether they reached 90% of their age-predicted maximal heart rate, which is calculated as $HR_{max} = 220 - Age(years)$ [30] [31]. While such heart-rate derived metrics are prevalent in research, their validity is subject to debate; age-based predictions do not account for individual fitness levels, physiological differences, or body composition and are influenced by variables like sleep [32] and caffeine consumption [33]. Consequently, unless heart rate is monitored within highly controlled settings, its use as a precise measure of workload is limited.

2.6. Statistics

2.6.1. Correlating with Established Fatigue Indicators: To explore the associations between fatigue metrics and established fatigue indicators such as heart rate, Respiratory Exchange Ratio (RER), and Borg's Ratings of Perceived Exertion (RPE) scale, the Kendall rank correlation coefficient was calculated (`scipy.stats.kendalltau`, version 1.11.3). Prior to conducting the Kendall rank correlation test, adjustments were made to ensure that each paired dataset was synchronized in time and equal in length, addressing the non-normal distribution of the residuals that were observed in the preliminary data analysis. The specific adjustments to the data for each metric to meet these requirements are as follows:

- Cosmed: breath-by-breath basis results in a variable sampling frequency, linear interpolation was used to achieve a consistent temporal distribution of samples. The data was then resampled to a uniform rate of either 1Hz or 2Hz, matching the frequency of the corresponding metric for analysis.
- RPE: recorded on a per-minute basis, remained at its original scale. Paired metrics for analysis were averaged into minute-wise bins to align with each RPE value.
- ARV: the data was already sampled at a consistent frequency of 2Hz suitable for further analysis without the need for additional resampling.
- IMDF and IMNF: the metrics were originally processed at 800Hz. The data was binned and averaged to create a 2Hz signal, harmonizing them with the lowest frequency component, namely the Cosmed data.
- FInsm5: the dataset was processed to a consistent sampling frequency of 1Hz. No further operations were needed for alignment.
- Entropy: the dataset was processed to a sampling frequency of 4Hz, and were averaged down to 2Hz. The data was then temporally aligned with the 2Hz Cosmed dataset, ensuring that each entropy measurement cluster corresponded with the appropriate Cosmed data points. These aligned data were then aggregated into a single dataset for each muscle.

		Participant				
System	**Muscle**	**p1**	**p2**	**p3**	**p4**	**p5**
Cosmed K5	N/A				m	
Polar HR band	N/A					
Delsys Avanti	GL_L	d			d	
	GM_L	d			d	
	TA_L	d				
	GL_R	-	-			
	GM_R	-	-			
	TA_R	-	-	m	m	m
RunWave	TA_R	m	m	-	-	-

TABLE I: Overview of Sensor Status Across Participants p1 through p5, detailing the presence (indicated by a blank cell), absence (-), detachment (d), or malfunction (m) for each sensor from the Cosmed, Polar HR, Delsys, and RunWave systems during the study.

2.6.2. Assessing sEMG Metric Variability in Response to Fatigue: In the examination of transitions between unfatigued and fatigued states within the collected fatigue metrics, the Wilcoxon signed-rank test was employed for its suitability in handling non-normal data distributions and within-subject comparisons. This non-parametric test effectively adjusts for inter-individual variability by concentrating on the median of paired differences, thereby isolating the effects of fatigue. The magnitude of the effect observed in the Wilcoxon signed-rank test was quantified using the rank-biserial correlation to provide a clearer understanding of the effect size.

For ARV data, the analysis required a distinct approach due to its expected non-linear behavior during exercise, typically rising initially before falling as fatigue develops. Generalized Additive Models (GAMs) were employed to capture this non-linear trend. Additionally, the coefficient of determination (R^2) was determined to evaluate the model's fit.

To reinforce the validity of the GAMs, bootstrapping methods were used to provide reliable confidence intervals for these non-linear estimations. This approach adeptly outlined the bidirectional patterns of ARV, identifying the peak before a subsequent decline indicative of fatigue.

Furthermore, to identify any statistically significant trends in the fatigue metrics, with the exception of the ARV, the Mann-Kendall trend test was applied specifically to data from the last two minutes of the protocol.

3. RESULTS

3.1. Participant Data Selection and Sensor Efficacy

Out of five initial participants, only three provided viable data (p2, p3, p5) due to sensor detachment and malfunctions (Table I). The analysis was thus confined to these individuals. Furthermore, the right Tibialis Anterior data was discarded for three participants due to consistent sensor issues.

The study focused on left leg recordings from the gastrocnemius lateralis, gastrocnemius medialis, and tibialis anterior muscles for the possible intra-limb muscular interactions.

3.2. Application and Durability of the RunWave

The custom-designed RunWave garment was trialed with participants 1 and 2 to gather sEMG data and evaluate its functional durability.

3.2.1. Participant 1 Experience: The initial application of the RunWave with Participant 1 revealed a significant weakness in the data acquisition board's resilience to the rigors of running. The intense ground contact motion caused a dislodgement of components on the circuit board, leading to system failure. Compounding this issue, the Delsys system sensors also detached from the participant's leg during this session. Despite this, the RunWave garment earned favorable feedback for its comfort; it was likened to standard compression wear, contrasting with the Delsys sensors that were reported to pull painfully at the skin before their detachment.

3.2.2. Post-Experiment Inspection and Participant 2 Trial: Subsequent inspection and repair involving the resoldering of detached components allowed for the second trial. Participant 2 was able to use the RunWave garment until a cable fatigue issue caused the wires from the lithium-ion battery to sever from the ESP32 microcontroller connector.

3.2.3. Assessment of RunWave Integrity: Further evaluation post-repair revealed that the initial dislodgement had caused irreparable internal damage to the circuit. This rendered the RunWave garment non-functional for subsequent experiments. These experiences highlighted the necessity for robust, movement-resistant design in wearable sEMG data acquisition systems, especially in high-motion contexts like running.

3.3. Validation fatigue inducement

In the study, volitional exhaustion served as the pivotal criterion for protocol termination, with each participant self-selecting their endpoint. Upon reaching this subjective limit, an RPE of 17 or greater was automatically assigned, indicative of a perceived level of exertion of 'very hard'. This self-determined cessation confirms the attainment of significant fatigue across all subjects. While all participants met most established markers for fatigue, the RER exceeding 1.10 was the sole exception, not achieved by every individual. Detailed data for all verification metrics can be found in the accompanying Table II. Graphical representation of the ventilatory thresholds, heart rate and respiratory exchange ratio per participant can be found in Appendix C.

Participant	**RPE$\geq$17**	**VT2**	**RER $\geq$ 1.10**	**90% HR$_{max}$**
p2	Yes	Yes	No	Yes
p3	Yes	Yes	No	Yes
p5	Yes	Yes	Yes	Yes

TABLE II: Overview of Fatigue Markers for Participants 2, 3, and 5. Indicates the presence ('Yes') or absence ('No') of fatigue markers RPE $\geq$ 17, VT2, RER $\geq$ 1.10, and $\geq 90\%$ HR$_{max}$ max for each participant

3.4. Correlating with Established Fatigue Indicators

Within this subsection, the results of the Kendall rank correlation tests are presented, focusing on the associations between sEMG-derived metrics and established fatigue indicators. The detailed correlation outcomes for one representative participant are displayed in Table III, while the comprehensive results for additional participants are included in Appendix A Table VIII for participant 3 and Table IX for participant 5.

3.4.1. Average Rectified Value: Across all participants, the ARV generally exhibits a positive correlation with HR, RER, and RPE. The correlation ranges from $0.36 < \tau < 0.66$ for participant 3, $0.43 < \tau < 0.73$ for participant 5. Participant 2, described in Table III, shows an anomaly having one muscle (GM_L) showing a statistically significant negative correlation with HR ($\tau = -0.22, p < 0.01$), RER ($\tau = -0.26, p < 0.01$) and RPE ($\tau = -0.4, p < 0.01$).

3.4.2. Instantaneous Mean and Median Frequency: The relationship between the IMDF, IMNF and the fatigue verification metrics does not follow an uniform pattern among participants, indicating a complex and individualized response during fatigue assessment. Notably, participant 2 exhibited a significant negative correlation in the gastrocnemius medialis (GM_L) muscle with both IMNF ($\tau = -0.57, p < 0.01$) and IMDF ($\tau = -0.6, p < 0.01$), and a similar negative trend was observed with IMDF in the tibialis anterior (TA_L) muscle ($\tau = -0.51, p < 0.01$). In contrast, participant 5 presented a substantial positive correlation for IMDF in the GM_L muscle ($\tau = 0.51, p < 0.01$), which could reflect an increase in frequency content.

3.4.3. Dimitrov's Spectral Fatigue index (FInsm5): The correlations for FInsm5 are mixed and generally weak across participants ranging from slightly negative to slightly positive. Participant 5's results were inconclusive, showing near-zero correlations across all validation metrics, suggesting that for this participant, the index does not significantly change with the state of fatigue as measured by HR, RER, and RPE.

3.4.4. Approximate and Sample Entropy: Both entropy metrics often show negative correlations with HR, RER, and RPE across participants, although this trend is not as strong and consistent as with ARV. Participant 2 demonstrated a negative correlation between ApEn and HR ($\tau = -0.33, p < 0.01$), and RER ($\tau = -0.27, p < 0.01$).

3.5. Assessing sEMG Metric Variability in Response to Fatigue

Within this subsection, we detail the outcomes of the Wilcoxon signed-rank tests, Generalized Additive Models (GAMs) with bootstrapping, and the Mann-Kendall trend test, highlighting the variability of sEMG metrics in response to fatigue. The analyses are organized by metric to discern significant intra-individual differences between fatigued and unfatigued states.

3.5.1. Wilcoxon signed-rank test: The results of the Wilcoxon signed-rank test and rank biserial correlation are summarized in Table IV. The p-values suggest that there are no statistically significant differences in the metrics between the fatigued and unfatigued state of the experiment, with each metric exceeding the conventional threshold for significance.

When considering the rank-biserial correlation values for effect size, a more nuanced picture emerges. The effect size

		HR		RER		RPE	
Metric	**Muscle**	τ	**p**	τ	**p**	τ	**p**
ARV	GL_L	0.7	<0.01	0.57	<0.01	0.77	<0.01
	GM_L	-0.22	<0.01	-0.26	<0.01	-0.4	0.05
	TA_L	0.34	<0.01	0.26	<0.01	0.32	0.12
IMNF	GLL	-0.07	<0.01	-0.06	<0.01	-0.09	0.67
	GM_L	-0.13	<0.01	-0.13	<0.01	-0.57	<0.01
	TA_L	-0.21	<0.01	-0.19	<0.01	-0.49	0.02
IMDF	GL_L	0.01	0.53	0.01	0.6	0.17	0.4
	GM_L	-0.09	<0.01	-0.09	<0.01	-0.6	<0.01
	TA_L	-0.1	<0.01	-0.09	<0.01	-0.51	0.01
FInsm5	GL_L	-0.3	<0.01	-0.3	<0.01	-0.64	<0.01
	GM_L	-0.46	<0.01	-0.4	<0.01	-0.7	<0.01
	TA_L	0.39	<0.01	0.28	<0.01	0.4	0.05
SampEn	GL_L	-0.33	<0.01	-0.26	<0.01	-0.36	0.12
	GM_L	-0.28	<0.01	-0.25	<0.01	-0.39	0.09
	TA_L	-0.39	<0.01	-0.3	<0.01	-0.46	0.05
ApEn	GL_L	-0.33	<0.01	-0.27	<0.01	-0.39	0.09
	GM_L	-0.29	<0.01	-0.26	<0.01	-0.39	0.09
	TA_L	-0.36	<0.01	-0.28	<0.01	-0.43	0.06

TABLE III: Results of Kendall Rank Correlation Test: Correlation coefficients (τ-value) and p-values between sEMG-based fatigue detection metrics (ARV, IMNF, IMDF, FInsm5, SampEn, ApEn) and fatigue verification metrics (HR, RER, RPE) for participant 2.

Metric	**W-statistic**	**p-value**	**Effect Size (r_{rb})**
IMNF	13.0	0.30	-0.42
IMDF	21.0	0.91	-0.07
FInsm5	10.0	0.16	-0.56
ApEn	11.0	0.20	-0.51
SampEn	12.0	0.25	-0.47

TABLE IV: Summary of Wilcoxon Signed-Rank Test Results and Effect Size for Five Metrics. This table presents the outcomes of the Wilcoxon Signed-Rank test, comparing fatigued and unfatigued conditions for each metric. The test statistic (W), p-values, and effect sizes (calculated using rank-biserial correlation) are shown for IMNF, IMDF, FInsm5, ApEn, and SampEn metrics

for IMNF (-0.42), ApEn (-0.51), and SampEn (-0.47) are moderate, indicating a notable, albeit not statistically significant, effect. The negative sign of the correlations suggests that the metrics tend to be lower in the fatigued condition, although the lack of statistical significance in the wilcoxon test indicates that this trend is not consistent across all participants or not strong enough to be deemed significant. It is noteworthy that the smallest effect size observed, of the IMDF, corresponds with the highest p-value, a pattern that aligns with typical expectations in statistical analysis.

3.5.2. Average Rectified Value: Generalized Additive Models: In-depth analysis of the ARV metric via Generalized Additive Models (GAMs) yielded high coefficients of determination, indicating excellent model fits for participant 2's GL_L ($R^2 = 0.97$), which displayed a pronounced increase to a maximum point, followed by a decline, a secondary peak, and a final drop before protocol termination. The GM_L ($R^2 = 0.76$) showed an initial rapid increase, a subsequent drop, and fluctuating behavior towards the end of the protocol. The TA_L ($R^2 = 0.94$) demonstrated a steady increase to a peak in the fourth stage, with intermittent dips followed by a decline.

		SampEn	ApEn	IMNF	IMDF	FInsm5
Participant	**Muscle**	**r-value**	**r-value**	**r-value**	**r-value**	**r-value**
p2	GL_L	-0.46**	-0.42**	0.01**	0.016**	-0.60**
	GM_L	-0.27**	-0.27**	$-1 \cdot 10^{-3}$	0.012**	0.01
	TA_L	0.04	0.13**	0.070**	0.066**	-0.40*
p3	GL_L	-0.09	0.04	0.027**	0.032**	-0.26
	GM_L	0.09	0.01	-0.042**	-0.040**	-0.73**
	TA_L	0.36**	0.29**	0.003	0.005*	0.69**
p5	GL_L	-0.05	0.04	$-1 \cdot 10^{-3}$	-0.002	-0.20
	GM_L	-0.16**	-0.18**	-0.003	0.007**	-0.11
	TA_L	-0.11*	-0.06	-0.039**	-0.047**	-0.27

TABLE V: Results of the Mann-Kendall Trend Test for participant p2, p3, and p5. For each muscle, the table details the `r-value` for five metrics. Significance indicated as follows: no stars () denote no significant trend, a single star (*) indicates a significance level of p<0.05, and two start (**) denotes significance of p<0.01.

Participant	**Muscle**	**R^2-value**	**R^2-CI**	**Figure Location**
p2	GL_L	0.97	0.96 - 0.97	Appendix D Figure 11a
	GM_L	0.76	0.73 - 0.79	Appendix D Figure 11b
	TA_L	0.94	0.92 - 0.95	Appendix D Figure 11c
p3	GL_L	0.95	0.94 - 0.06	Appendix D Figure 12a
	GM_L	0.87	0.84 - 0.89	Appendix D Figure 12b
	TA_L	0.98	0.97 - 0.98	Appendix D Figure 12c
p5	GL_L	0.97	0.96 - 0.97	Appendix D Figure 13a
	GM_L	0.79	0.77 - 0.81	Appendix D Figure 13b
	TA_L	0.99	0.98 - 0.99	Appendix D Figure 13c

TABLE VI: Results of the ARV GAM models for participant 2, 3, and 5. For each muscle, the table details the coefficient of determination (R^2), the confidence interval, and the location where the Figures are located.

Participant 3's ($R^2 = 0.95$) exhibited a sharp initial increase, a slight dip, and then a less steep rise to a high point before a consistent decline. The GM_L ($R^2 = 0.87$) showed a gradual increase with small dips, peaking significantly in the final incremental stage before declining. The TA_L ($R^2 = 0.98$) increased rapidly, dipped, rose again, and then oscillated before a final decline.

For participant 5, the GL_L ($R^2 = 0.97$) revealed a rapid initial increase that leveled off and peaked at stage 5, followed by a slow decrease and fluctuations before termination. The GM_L ($R^2 = 0.79$) demonstrated fluctuating behavior throughout, with a notable peak at stage 7. The TA_L ($R^2 = 0.99$), described in Figure 5, showed a clear increase, a secondary peak in stage 8, and a decline towards the end.

4. Discussion

This study aimed to explore the intricate dynamics of muscle fatigue in the context of incremental treadmill running tests, employing metrics such as entropy, Average Rectified Value (ARV), heart rate (HR), metabolic equivalents (METS), mean and median frequencies, and the Spectral Fatigue Index (FInsm5) for a comprehensive analysis.

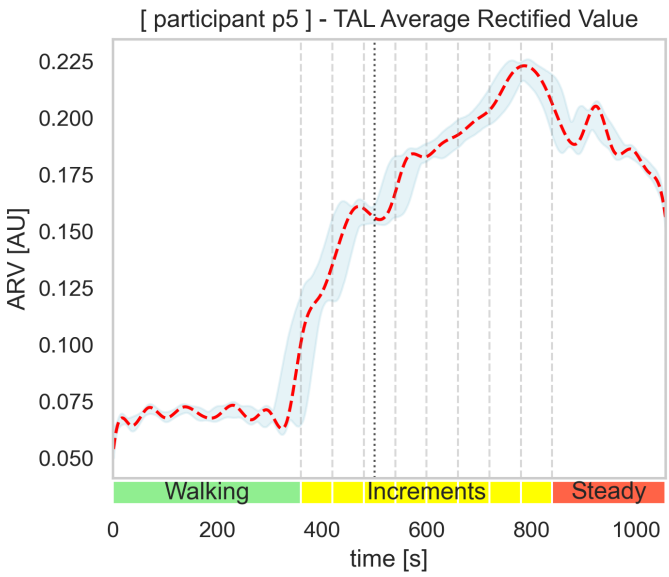

Fig. 5: General Additive Model: Average Rectified Value (ARV) Analysis for Participant 5's Tibialis Anterior Muscle Across Experiment Stages

4.1. RunWave Garment

4.1.1. Fitment Considerations: A critical aspect in the design of the RunWave involves ensuring the precise fitment to optimize electrode-skin contact and accurate placement over the targeted muscle groups. The garment's sizing is crucial to minimize any movement of the electrodes and maintain their proper alignment above the muscles.

Unlike traditional gelled electrodes, textile electrodes used in the RunWave are larger, offering a degree of flexibility in placement. However, this also introduces challenges in creating an universal fit. The anatomical diversity among individuals, especially concerning the length from the ankle to the knee joint and the circumference of the triceps surae, necessitates the production of multiple garment sizes.

In the initial design phase, I developed three distinct sizes: small, medium, and large. These sizes were determined based on the circumference measurements at two key points: the largest circumference of the triceps surae and just below the gastrocnemius muscle heads. This approach was intended to accommodate the variance in muscle size and shape for a better fit.

However, it became evident that a more adaptable material is required. The ideal fabric would possess high elasticity to conform to a broader range of lower leg sizes while maintaining sufficient tension to secure the garment in place. Such an improvement in the material would enhance the garment's versatility, making it more accommodating to different body types without compromising the efficacy of the electrode placement.

4.1.2. Electronic Limitations: One of the primary challenges encountered in the development of the RunWave garment's electronics was the limited capability of the ESP32's 12-bit Analog-to-Digital Converter (ADC). This limitation necessitated the implementation of hardware filtering and amplification to enhance signal quality. The initial objective was to simultaneously capture the activity of three muscles: the gastrocnemius medialis, gastrocnemius lateralis, and tibialis anterior. However, due to the constraints in size, which was a necessary consideration for mounting the device on the leg, the design was limited to a single-channel setup.

A higher-resolution ADC could have potentially addressed this issue. Nevertheless, the challenge extended to the availability and suitability of components. The high-resolution ADCs readily available in the market are typically designed for applications requiring high precision but at lower frequencies. These components usually offer a maximum sampling frequency of 400-800Hz for 16 to 24-bit ADCs, which was not adequate for our requirements.

Post-design reflections revealed that it might have been feasible to directly integrate an ESP32 System on Chip (SoC) on a custom Printed Circuit Board (PCB), along with a surface-mounted device (SMD) based higher-resolution ADC. Such an ADC could meet the required sampling frequencies. However, integrating these components exceeded the scope of this research project due to their complexity and the need for extensive redesign.

Another electronic consideration was the power management system. The intention was to utilize the onboard power management feature of the ESP32 system, powered by a lithium-ion battery. However, the system's maximum voltage output of 3.2/3.3 volts imposed further constraints on the selection of appropriate operational amplifiers (op-amps) for the circuit.

4.2. Inducement of Fatigue and Experimental Design

The study faced significant challenges in validating fatigue due to the diverse backgrounds and varying familiarity of participants with treadmill running and sensor-equipped exercise. This diversity was reflected in the substantial cardiorespiratory differences observed among participants, as evidenced by the varied points at which they reached their ventilatory thresholds (VT1 and VT2). The figures can be found in Appendix C Figure 8, 9, and 10.

For example, while Participant 2 reached VT1 during the walking phase and VT2 just before the experiment's termination, Participant 3 attained these thresholds at different stages of the incremental exercise. Such variations highlight the necessity of a more refined participant selection process. A targeted approach should be considered, focusing on factors such as active monthly/weekly running distances and average times per kilometer for a 5km run. This would ensure a group with closer similarities in terms of current running status and performance, thereby reducing variability in the results.

Moreover, the unfamiliarity of some participants with treadmill running and the experimental setup was a notable factor contributing to the variability in the study. Participants who were competitive runners, like Participants 3 and 5, tended to push beyond their second ventilatory threshold, indicating a disparity in response between active and less active runners.

To mitigate these challenges, introducing a two-session approach could be beneficial. The first session would aim to

familiarize participants with the treadmill running environment and the sensor equipment. This session could also be used to determine the optimal velocity for the constant velocity stage of the experiment, ensuring that the protocol is better tailored to each individual. This approach would not only acclimatize participants to the experimental conditions but also allow for a more accurate assessment of their performance and fatigue levels.

4.3. Local Fatigue Metrics versus Systemic Fatigue Indicators

Across all participants, the correlations of HR and RER with the fatigue metrics were notably high in terms of significance, with 16 to 17 out of 18 muscles showing significant correlations. However, it's important to note that while these correlations were numerous, they were relatively low in magnitude.

In contrast, the RPE scale, despite showing a decrease in the number of significant correlations (7 to 10 out of 18), demonstrated higher magnitudes in correlation coefficients. This difference suggests that while HR and RER are effective systemic markers of cardiorespiratory fatigue, capturing the body's metabolic state, RPE provides a more nuanced view. RPE, being a subjective metric, likely encompasses not only systemic fatigue but also the sensations of localized muscle fatigue and other discomforts.

The ARV emerged as the metric with the highest correlation across participants. This finding underscores the importance of measuring multiple muscles simultaneously, as local muscle fatigue often precedes systemic fatigue indicated by cardiorespiratory markers. The onset of localized muscle fatigue typically occurs earlier during exercise, potentially leading to altered movement patterns as the body redistributes effort to less fatigued muscles.

In fatigue research, the addition of movement data to analyze strategies and alterations is of paramount importance. This approach is crucial because the markers of systemic fatigue, such as heart rate (HR) and respiratory exchange ratio (RER), do not necessarily coincide with the onset or presence of localized muscle fatigue. A muscle can exhibit signs of fatigue while systemic indicators suggest a normal state, and conversely, systemic fatigue may be present without localized muscle fatigue.

This disconnect underscores the limitations of relying solely on systemic fatigue markers to understand the full spectrum of fatigue. In light of this, our study emphasizes the need for a holistic analysis that not only considers systemic indicators but also closely examines muscle synergy and movement patterns. By doing so, we can gain deeper insights into how fatigue affects the body both systemically and at a localized level, revealing potential movement adaptations that occur as a response to muscle fatigue.

Such an integrated approach is instrumental in accurately identifying and understanding the complexities of fatigue, especially in dynamic activities like running. It enables a more nuanced assessment of fatigue, capturing the intricate interplay between systemic physiological responses and the specific demands placed on individual muscle groups.

4.4. Assessing Muscle Fatigue

In our study, the assessment of muscle fatigue through advanced metrics revealed several key insights. A notable finding was the lack of significant differentiation between fatigued and unfatigued conditions, likely attributable to the use of a non-parametric test. Non-parametric tests, which do not assume a specific data distribution, are often used in small sample sizes like ours. Despite the moderate effect size observed, the insignificant results were expected given the small cohort of only three participants, thus limiting the ability to draw consistent conclusions.

The computational demands of calculating the IMNF and IMDF were substantial. We anticipated differences of 1-3 Hz between fatigued and unfatigued states, but these were not detectable in our post-exercise analysis. Consequently, the use of IMNF or IMDF for real-time or near real-time analysis on a low-power microsystem appears impractical. However, their utility might improve when applied to per gait cycle analysis.

When comparing IMNF, IMDF with the FInsm5, FInsm5 demonstrated a better capacity for distinguishing between fatigued and unfatigued states. It showed the lowest, albeit not insignificant, p-value and the highest effect size in the Wilcoxon signed-rank test (Table IV), along with significant trends in the Mann-Kendall trend test (Table V). However, it's important to note that the results were not consistent across participants.

Among all metrics evaluated, the ARV stood out for its simplicity and ease of calculation. It demonstrated a clear temporal response to exercise intensity, typically increasing during submaximal exercise and showing either a decrement or a clear sign of resource reallocation or adaptation when the intensity could no longer be maintained. ARV correlated relatively highly with HR, RER, and RPE. Notably, the expected behavior of ARV diverges from these cardiorespiratory and subjective markers once fatigue sets in, as both HR and RPE tend to increase and level off, whereas ARV either plateaus earlier (if the muscle maintains the level of excitation) or drops. This discrepancy results in a reduction in the expected correlation between ARV and HR/RPE.

The ARV stands out as the ideal fatigue metric for the RunWave garment, particularly due to its use of textile-based electrodes. These electrodes, more practical for dynamic sports, lack the precision of traditional silver gelled electrodes, making ARV's simplicity and computational efficiency key advantages. ARV effectively signals muscle fatigue and resource reallocation, maintaining reliability despite the textile electrodes' lower signal fidelity. Its integration into the RunWave garment harnesses these strengths, offering athletes accurate, real-time fatigue feedback in an user-friendly format, essential for endurance sports.

5. CONCLUSION

The RunWave smart garment, designed for detecting fatigue during running outside of laboratory settings, has shown promising yet mixed results. The garment's potential for practical application in real-world scenarios has been assessed based on several key factors.

The difficulty in designing an one-size-fits-all device was apparent. The garment faced challenges in fitment, as it needed to cater to diverse body types and sizes, which is crucial for proper electrode placement and effective data collection.

The device was limited to monitoring a single muscle due to electronic constraints and size limitations, which narrowed its scope of fatigue detection. Furthermore, the garment's malfunction during intense running highlighted the need for a more robust design to withstand the rigors of outdoor sports.

Despite these challenges, the feedback from participants was overwhelmingly positive. They found the RunWave garment more comfortable and less intrusive compared to traditional sensors like Delsys. It was experienced as a regular compression garment, enhancing its suitability for everyday athletic use.

With targeted improvements to address these issues, the RunWave garment holds the potential to effectively meet its goal of fatigue detection during outdoor running. This includes refining the fitment, enhancing the durability of the electronics, and possibly expanding its capability to monitor multiple muscles.

The ARV emerged as the most suitable metric for this application. Its simplicity, computational efficiency, and clear correlation with muscle fatigue, even with textile-based electrodes, make it an ideal choice for real-time analysis in the RunWave garment.

The study suggests that monitoring a single muscle may not suffice for comprehensive fatigue detection, as movement alterations and varying exercise intensities can redistribute muscle effort. Therefore, it's advantageous to monitor dominant muscle groups that are actively engaged in the running activity. With textile electrodes, it is feasible to cover larger areas, such as both gastrocnemius muscles simultaneously, providing a easier view of muscle activity. The diversity among individuals further supports the need for a multi-muscle monitoring approach to accurately identify the 'weakest link' in terms of fatigue.

In conclusion, the RunWave smart garment, with its innovative approach and user-friendly design, demonstrates potential as a tool for outdoor fatigue detection in running. By addressing its current limitations and harnessing the strengths of ARV as a fatigue metric, the garment can be refined to effectively monitor and analyze muscle excitation, paving the way for more personalized and dynamic fatigue assessment in endurance sports.

REFERENCES

[1] D. Micklewright, A. St Clair Gibson, V. Gladwell, and A. Al Salman. Development and Validity of the Rating-of-Fatigue Scale. *Sports Medicine*, 47(11):2375–2393, 11 2017.

[2] Brian Forsythe, Derrick M. Knapik, Matthew D. Crawford, Connor C. Diaz, David Hardin, John Gallucci, Holly Jacinda Silvers-Granelli, Bert R. Mandelbaum, Lawrence Lemak, Margot Putukian, and Eric Giza. Incidence of Injury for Professional Soccer Players in the United States: A 6-Year Prospective Study of Major League Soccer. *Orthopaedic Journal of Sports Medicine*, 10(3):232596712110551, 3 2022.

[3] Koen Jongbloed. Defining and measuring fatigue in endurance sports. Technical report, TU Delft, 2022.

[4] Edward A. Clancy, Evelyn L. Morin, Gelareh Hajian, and Roberto Merletti. Tutorial. Surface electromyogram (sEMG) amplitude estimation: Best practices. *Journal of Electromyography and Kinesiology*, 72:102807, 10 2023.

[5] Alan Oppenheim, Alan Wilsky, and Syed Nawab. *Signals and Systems*. Pearson Education Limited, second edition edition, 2014.

[6] GEORGE V. DIMITROV, TODOR I. ARABADZHIEV, KATYA N. MILEVA, JOANNA L. BOWTELL, NICOLA CRICHTON, and NONNA A. DIMITROVA. Muscle Fatigue during Dynamic Contractions Assessed by New Spectral Indices. *Medicine & Science in Sports & Exercise*, 38(11):1971–1979, 11 2006.

[7] Stacey A. Meardon, Joseph Hamill, and Timothy R. Derrick. Running injury and stride time variability over a prolonged run. *Gait & Posture*, 33(1):36–40, 1 2011.

[8] Python Software Foundation. Python, 2023.

[9] Milad Alizadeh-Meghrazi, Binbin Ying, Alessandra Schlums, Emily Lam, Ladan Eskandarian, Farhana Abbas, Gurjant Sidhu, Amin Mahnam, Bastien Moineau, and Milos R. Popovic. Evaluation of dry textile electrodes for long-term electrocardiographic monitoring. *BioMedical Engineering OnLine*, 20(1):68, 7 2021.

[10] A Shafti, R B Ribas Manero, A M Borg, K Althoefer, and M J Howard. Embroidered Electromyography: A Systematic Design Guide. *IEEE Transactions on Neural Systems and Rehabilitation Engineering*, 25(9):1472–1480, 2017.

[11] Emily Lam, Milad Alizadeh-Meghrazi, Alessandra Schlums, Ladan Eskandarian, Amin Mahnam, Bastien Moineau, and Milos R Popovic. Exploring textile-based electrode materials for electromyography smart garments. *Journal of Rehabilitation and Assistive Technologies Engineering*, 9:205566832110619, 1 2022.

[12] Hermie J Hermens, Bart Freriks, Catherine Disselhorst-Klug, and Günter Rau. Development of recommendations for SEMG sensors and sensor placement procedures. *Journal of Electromyography and Kinesiology*, 10(5):361–374, 10 2000.

[13] Bernabe Rodriguez-Tapia, Israel Soto, Daniela M. Martinez, and Norma Candolfi Arballo. Myoelectric Interfaces and Related Applications: Current State of EMG Signal Processing–A Systematic Review. *IEEE Access*, 8:7792–7805, 2020.

[14] Michael McKnight, Talha Agcayazi, Tushar Ghosh, and Alper Bozkurt. Fiber-Based Sensors. In *Wearable Technology in Medicine and Health Care*, pages 153–171. Elsevier, 2018.

[15] Jingpeng Wang, Liqiong Tang, and John E Bronlund. Surface EMG Signal Amplification and Filtering. *International Journal of Computer Applications*, 82(1):15–22, 11 2013.

[16] Andrew D. Vigotsky, Israel Halperin, Gregory J. Lehman, Gabriel S. Trajano, and Taian M. Vieira. Interpreting Signal Amplitudes in Surface Electromyography Studies in Sport and Rehabilitation Sciences. *Frontiers in Physiology*, 8, 1 2018.

[17] R B Ribas Manero, A Shafti, B Michael, J Grewal, J Ll Ribas Fernandez, K Althoefer, and M J Howard. Wearable embroidered muscle activity sensing device for the human upper leg. *Annual International Conference of the IEEE Engineering in Medicine and Biology Society. IEEE Engineering in Medicine and Biology Society. Annual International Conference*, 2016:6062–6065, 8 2016.

[18] M González-Izal, A Malanda, E Gorostiaga, and M Izquierdo. Electromyographic models to assess muscle fatigue. *Journal of Electromyography and Kinesiology*, 22(4):501–512, 2012.

[19] Jing-jing Wan, Zhen Qin, Peng-yuan Wang, Yang Sun, and Xia Liu. Muscle fatigue: general understanding and treatment. *Experimental & Molecular Medicine*, 49(10):e384–e384, 10 2017.

[20] Samuel C. K. Lee, David W. Russ, and Stuart A. Binder-Macleod. Force-Frequency Relation of Skeletal Muscle. In *Encyclopedia of Neuroscience*, pages 1608–1611. Springer Berlin Heidelberg, Berlin, Heidelberg.

[21] D. G. Allen, G. D. Lamb, and H. Westerblad. Skeletal Muscle Fatigue: Cellular Mechanisms. *Physiological Reviews*, 88(1):287–332, 1 2008.

[22] F. Molinari, M. Knaflitz, P. Bonato, and M.V. Actis. Electrical Manifestations of Muscle Fatigue During Concentric and Eccentric Isokinetic Knee Flexion-Extension Movements. *IEEE Transactions on Biomedical Engineering*, 53(7):1309–1316, 7 2006.

[23] K. Schneider and M. Farge. Wavelets: Mathematical Theory. In *Encyclopedia of Mathematical Physics*, pages 426–438. Elsevier, 2006.

[24] K H Schütte, E A Maas, V Exadaktylos, D Berckmans, R E Venter, and B Vanwanseele. Wireless tri-axial trunk accelerometry detects deviations in dynamic center of mass motion due to running-induced fatigue. *PLoS ONE*, 10(10), 2015.

[25] Kurt H Schütte, Stefan Seerden, Rachel Venter, and Benedicte Vanwanseele. Influence of outdoor running fatigue and medial tibial stress syndrome on accelerometer-based loading and stability. *Gait & posture*, 59:222–228, 1 2018.

[26] Steven Strogatz. *Nonlinear Dynamics and Chaos*. Westview Press, second edition edition, 2015.

[27] Jennifer M. Yentes, Nathaniel Hunt, Kendra K. Schmid, Jeffrey P. Kaipust, Denise McGrath, and Nicholas Stergiou. The Appropriate Use of Approximate Entropy and Sample Entropy with Short Data Sets. *Annals of Biomedical Engineering*, 41(2):349–365, 2 2013.

[28] Nerys Williams. The Borg Rating of Perceived Exertion (RPE) scale. *Occupational Medicine*, 67(5):404–405, 7 2017.

[29] K N Radzak and C D Stickley. Fatigue-induced hip-abductor weakness and changes in biomechanical risk factors for running-related injuries. *Journal of Athletic Training*, 55(12):1270–1276, 2020.

[30] Z Gao, Q Mei, G Fekete, J S Baker, and Y Gu. The effect of prolonged running on the symmetry of biomechanical variables of the lower limb joints. *Symmetry*, 12(5), 2020.

[31] B Bazuelo-Ruiz, J V Durá-Gil, N Palomares, E Medina, and S Llana-Belloch. Effect of fatigue and gender on kinematics and ground reaction forces variables in recreational runners. *PeerJ*, 2018(3), 2018.

[32] Louis Faust, Keith Feldman, Stephen M. Mattingly, David Hachen, and Nitesh V. Chawla. Deviations from normal bedtimes are associated with short-term increases in resting heart rate. *npj Digital Medicine*, 3(1):39, 12 2020.

[33] Luana Almeida Gonzaga, Luiz Carlos Marques Vanderlei, Rayana Loch Gomes, and Vitor Engrácia Valenti. Caffeine affects autonomic control of heart rate and blood pressure recovery after aerobic exercise in young adults: a crossover study. *Scientific reports*, 7(1):14091, 2017.

APPENDIX A
RESULTS: STATISTICAL ANALYSIS TABLES

		HR		RER		RPE	
Metric	**Muscle**	τ	**p**	τ	**p**	τ	**p**
ARV	GL_L	0.7	<0.01	0.57	<0.01	0.77	<0.01
	GM_L	-0.22	<0.01	-0.26	<0.01	-0.4	0.05
	TA_L	0.34	<0.01	0.26	<0.01	0.32	0.12
IMNF	GL_L	-0.07	<0.01	-0.06	<0.01	-0.09	0.67
	GM_L	-0.13	<0.01	-0.13	<0.01	-0.57	<0.01
	TA_L	-0.21	<0.01	-0.19	<0.01	-0.49	0.02
IMDF	GL_L	0.01	0.53	0.01	0.6	0.17	0.4
	GM_L	-0.09	<0.01	-0.09	<0.01	-0.6	<0.01
	TA_L	-0.1	<0.01	-0.09	<0.01	-0.51	0.01
FInsm5	GL_L	-0.3	<0.01	-0.3	<0.01	-0.64	<0.01
	GM_L	-0.46	<0.01	-0.4	<0.01	-0.7	<0.01
	TA_L	0.39	<0.01	0.28	<0.01	0.4	0.05
SampEn	GL_L	-0.33	<0.01	-0.26	<0.01	-0.36	0.12
	GM_L	-0.28	<0.01	-0.25	<0.01	-0.39	0.09
	TA_L	-0.39	<0.01	-0.3	<0.01	-0.46	0.05
ApEn	GL_L	-0.33	<0.01	-0.27	<0.01	-0.39	0.09
	GM_L	-0.29	<0.01	-0.26	<0.01	-0.39	0.09
	TA_L	-0.36	<0.01	-0.28	<0.01	-0.43	0.06

TABLE VII: Correlation coefficients (τ) and p-values indicating the strength and significance of the relationships between various sEMG-based fatigue detection metrics (ARV, IMNF, IMDF, FInsm5, SampEn, ApEn) and fatigue verification metrics (HR, RER, RPE) for participant 2.

		HR		RER		RPE	
Metric	**Muscle**	τ	**p**	τ	**p**	τ	**p**
ARV	GL_L	0.56	<0.01	0.53	<0.01	0.63	<0.01
	GM_L	0.36	<0.01	0.51	<0.01	0.35	0.03
	TA_L	0.59	<0.01	0.59	<0.01	0.66	<0.01
IMNF	GL_L	-0.05	<0.01	-0.05	<0.01	-0.3	0.07
	GM_L	0.05	<0.01	0.06	<0.01	0.3	0.07
	TA_L	0.01	0.39	-0.01	0.54	0.07	0.69
IMDF	GL_L	0.03	0.02	0.03	0.02	0.08	0.64
	GM_L	0.07	<0.01	0.07	<0.01	0.31	0.06
	TA_L	0.03	0.07	0.0	0.8	0.13	0.43
FInsm5	GL_L	-0.4	<0.01	-0.14	<0.01	-0.52	<0.01
	GM_L	0.53	<0.01	0.4	<0.01	0.63	<0.01
	TA_L	0.08	<0.01	-0.08	<0.01	0.18	0.29
SampEn	GL_L	-0.32	<0.01	-0.27	<0.01	-0.42	0.05
	GM_L	-0.15	<0.01	-0.12	<0.01	-0.39	0.07
	TA_L	0.37	<0.01	0.35	<0.01	0.34	0.12
ApEn	GL_L	-0.6	<0.01	-0.45	<0.01	-0.66	<0.01
	GM_L	-0.12	<0.01	-0.1	<0.01	-0.26	0.24
	TA_L	0.05	0.05	0.08	<0.01	-0.12	0.58

TABLE VIII: Correlation coefficients (τ) and p-values indicating the strength and significance of the relationships between various sEMG-based fatigue detection metrics (ARV, IMNF, IMDF, FInsm5, SampEn, ApEn) and fatigue verification metrics (HR, RER, RPE) for participant 3.

		HR		RER		RPE	
Metric	**Muscle**	τ	**p**	τ	**p**	τ	**p**
ARV	GL_L	0.54	<0.01	0.47	<0.01	0.55	<0.01
	GM_L	0.52	<0.01	0.43	<0.01	0.73	<0.01
	TA_L	0.61	<0.01	0.59	<0.01	0.65	<0.01
IMNF	GL_L	-0.04	<0.01	-0.03	0.03	-0.46	0.01
	GM_L	0.05	<0.01	0.04	<0.01	0.41	0.02
	TA_L	0.02	0.14	0.02	0.18	-0.14	0.43
IMDF	GL_L	0.05	<0.01	0.05	<0.01	0.0	1.0
	GM_L	0.05	<0.01	0.06	<0.01	0.51	<0.01
	TA_L	0.03	0.07	0.02	0.24	-0.08	0.64
FInsm5	GL_L	-0.34	<0.01	-0.3	<0.01	-0.56	<0.01
	GM_L	0.04	0.04	0.06	0.01	-0.01	0.94
	TA_L	0.28	<0.01	0.4	<0.01	0.31	0.09
SampEn	GL_L	-0.22	<0.01	-0.09	<0.01	-0.31	0.13
	GM_L	0.26	<0.01	0.23	<0.01	0.31	0.13
	TA_L	0.43	<0.01	0.44	<0.01	0.48	0.02
ApEn	GL_L	-0.66	<0.01	-0.49	<0.01	-0.85	<0.01
	GM_L	-0.05	0.05	-0.04	0.13	-0.06	0.78
	TA_L	0.27	<0.01	0.27	<0.01	0.62	<0.01

TABLE IX: Correlation coefficients (τ) and p-values indicating the strength and significance of the relationships between various sEMG-based fatigue detection metrics (ARV, IMNF, IMDF, FInsm5, SampEn, ApEn) and fatigue verification metrics (HR, RER, RPE) for participant 5.

		SampEn		ApEn		IMNF		IMDF		FInsm5	
Participant	**Muscle**	**r-value**	**p-value**	**r-value**	**p-value**	**r-value**	**p-value**	**r-value**	**p-value**	**r-value**	**p-value**
p2	GL_L	-0.46	<0.01	-0.42	<0.01	0.01	<0.01	0.016	<0.01	-0.60	<0.01
	GM_L	-0.27	<0.01	-0.27	<0.01	$-1 \cdot 10^{-3}$	0.79	0.012	<0.01	0.01	1.0
	TA_L	0.04	0.16	0.13	<0.01	0.070	<0.01	0.066	<0.01	-0.40	0.02
p3	GL_L	-0.09	0.16	0.04	0.56	0.027	<0.01	0.032	<0.01	-0.26	0.15
	GM_L	0.09	0.14	0.01	0.88	-0.042	<0.01	-0.040	<0.01	-0.73	<0.01
	TA_L	0.36	<0.01	0.29	<0.01	0.003	0.18	0.005	0.04	0.69	<0.01
p5	GL_L	-0.05	0.35	0.04	0.51	0	0.85	-0.002	0.28	-0.20	0.26
	GM_L	-0.16	0.004	-0.18	<0.01	-0.003	0.16	0.007	<0.01	-0.11	0.54
	TA_L	-0.11	0.048	-0.06	0.27	-0.039	<0.01	-0.047	<0.01	-0.27	0.13

TABLE X: Mann-Kendall trend test results showing correlation coefficients (r-values) and associated p-values for Sample Entropy (SampEn), Approximate Entropy (ApEn), Instantaneous Mean Frequency (IMNF), Instantaneous Median Frequency (IMDF), and the Spectral Fatigue Index (FInsm5) across three participants (p2, p3, p5) for different muscles (Gastrocnemius Lateralis - GL_L, Gastrocnemius Medialis - GM_L, Tibialis Anterior - TA_L). Significance levels are indicated with p-values, where values less than 0.01 are considered highly significant.

APPENDIX B
ELECTRONICS

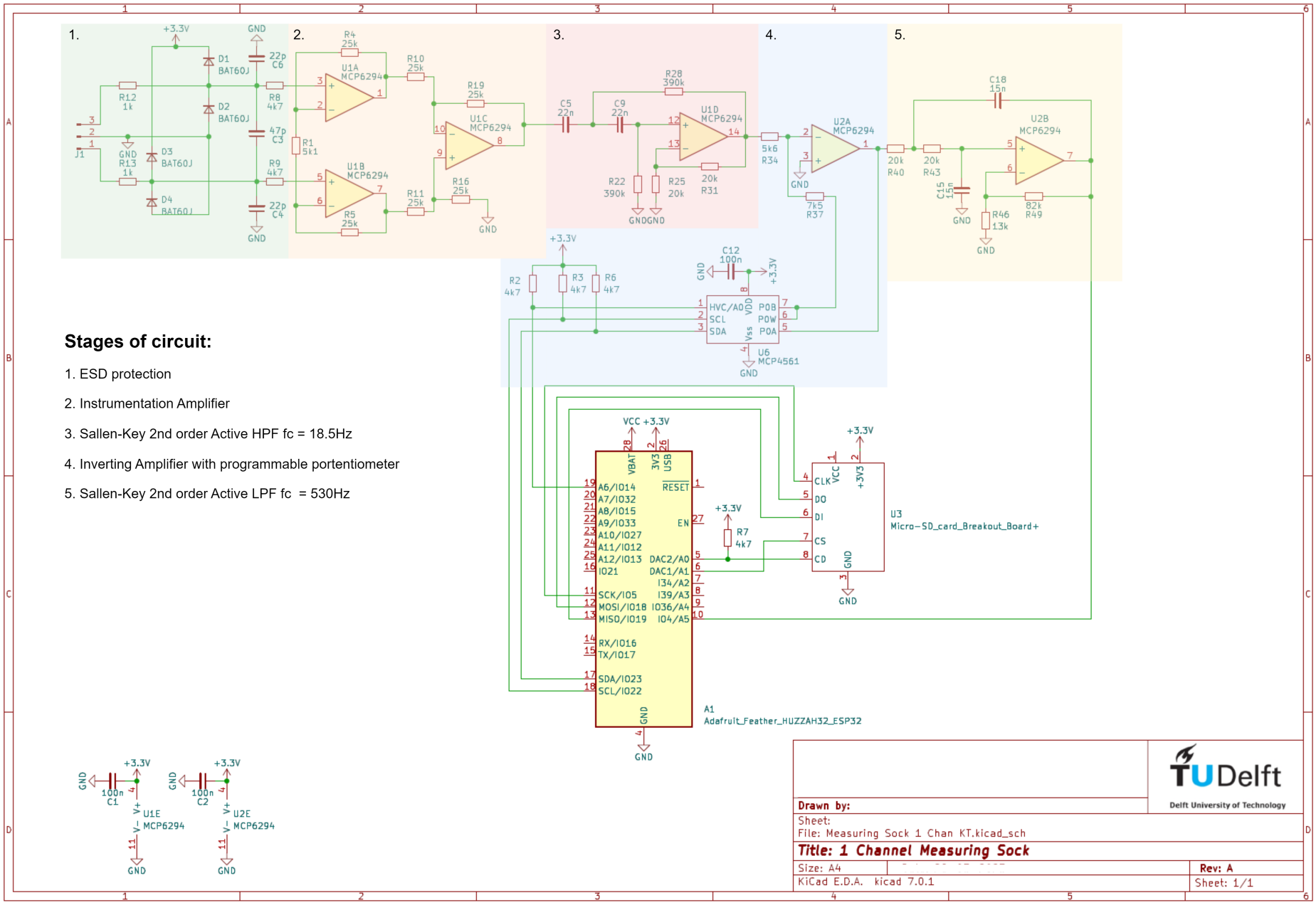

Fig. 6: Circuit containing four stage amplification and filtering system for surface electromyography data acquisition.

2. Instrumentation Amplifier

$$G_{inst} = \frac{1 + (R_4 + R_5)}{R_{gain}}$$

$$G_{inst} = \frac{1 + (25 * 10^3 + 25 * 10^3)}{5.1 * 10^3} = 10.81$$

3. Sallen-Key HPF

$$f_c = \frac{1}{2\pi \cdot \sqrt{R_{28} \cdot R_{22} \cdot C_5 \cdot C_9}}, R_{28} = R_{22} || C_5 = C_9$$

$$f_c = \frac{1}{2\pi \cdot R_{28} \cdot C_5} = \frac{1}{2\pi \cdot 390 \cdot 10^3 \cdot 22 \cdot 10^{-9}} = 18.5Hz$$

$$G_{HPF} = 1 + \frac{R_{31}}{R_{25}} = 1 + \frac{20 \cdot 10^3}{20 \cdot 10^3} = 2$$

4. Inverting Adjustable Amp

$$G_{inv} = \frac{R_{37} + R_{potentiometer}}{R_{34}}$$

$$G_{invMIN} = \frac{7.5 \cdot 10^3 + 0}{5.6 \cdot 10^3} = 1.34$$

$$G_{invMAX} = \frac{7.5 \cdot 10^3 + 100 \cdot 10^3}{5.6 \cdot 10^3} = 19.20$$

Rpot adjustable in 255 steps between 0-100kohm

5. Sallen-Key LPF

$$f_c = \frac{1}{2\pi \cdot \sqrt{R_{40} \cdot R_{43} \cdot C_{18} \cdot C_{15}}}, R_{40} = R_{43} || C_{18} = C_{15}$$

$$f_c = \frac{1}{2\pi \cdot R_{40} \cdot C_{18}} = \frac{1}{2\pi \cdot 20 \cdot 10^3 \cdot 15 \cdot 10^{-9}} = 530Hz$$

$$G_{LPF} = 1 + \frac{R_{49}}{R_{46}} = 1 + \frac{82 \cdot 10^3}{13 \cdot 10^3} = 7.31$$

Fig. 7: Calculations for the four stage amplification and filtering circuit.

APPENDIX C
VISUALIZATIONS: CARDIORESPIRATORY DATA

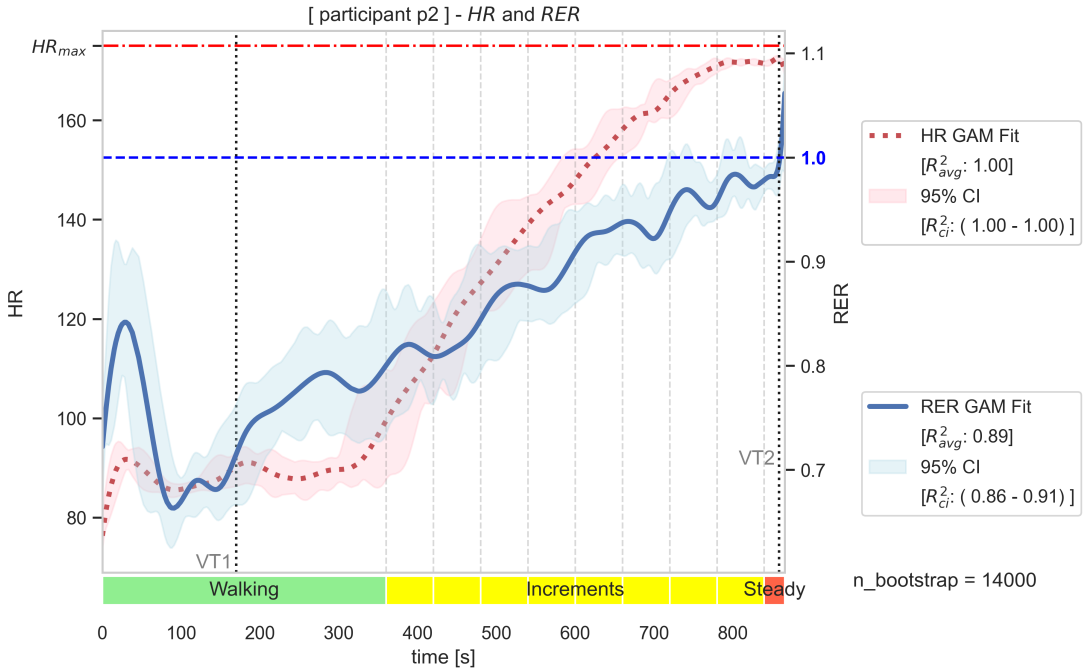

Fig. 8: Cardiorespiratory data participant 2. Visualization of GAM fit with CI by bootstrapping of heart rate (HR) and Respiratory Exchange Ratio (RER) versus time. Horizontal colorcoding indicates the walking stage, increment stages, and the steady velocity stage. The start and end of each increment stage is marked with a gray striped vertical line. Horizontal striped blue line indicates RER = 1.0 and determines the point of the ventilatory threshold 2 (VT2). The horizontal striped red line indicates the age-based maximum heart rate.

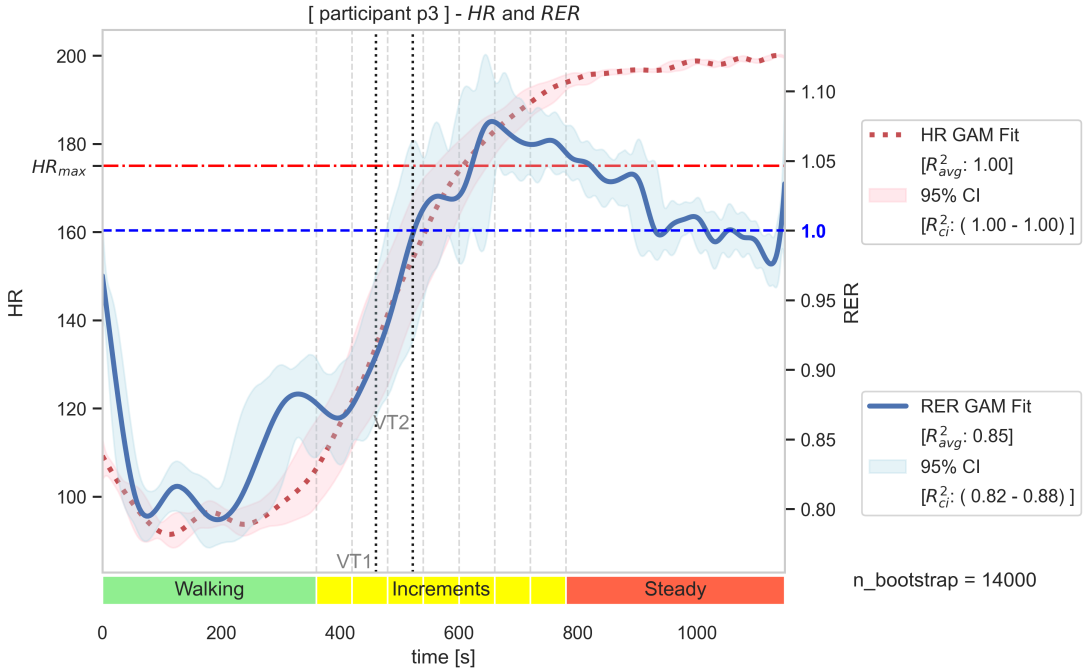

Fig. 9: Cardiorespiratory data participant 3. Visualization of GAM fit with CI by bootstrapping of heart rate (HR) and Respiratory Exchange Ratio (RER) versus time. Horizontal colorcoding indicates the walking stage, increment stages, and the steady velocity stage. The start and end of each increment stage is marked with a gray striped vertical line. Horizontal striped blue line indicates RER = 1.0 and determines the point of the ventilatory threshold 2 (VT2). The horizontal striped red line indicates the age-based maximum heart rate.

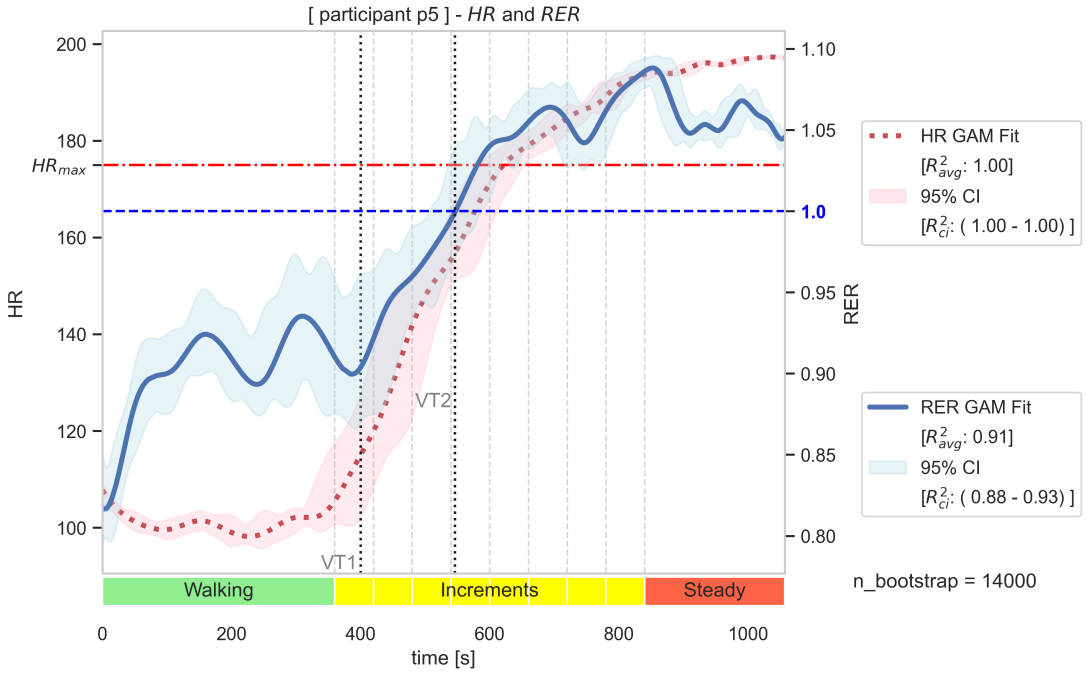

Fig. 10: Cardiorespiratory data participant 5. Visualization of GAM fit with CI by bootstrapping of heart rate (HR) and Respiratory Exchange Ratio (RER) versus time. Horizontal colorcoding indicates the walking stage, increment stages, and the steady velocity stage. The start and end of each increment stage is marked with a gray striped vertical line. Horizontal striped blue line indicates RER = 1.0 and determines the point of the ventilatory threshold 2 (VT2). The horizontal striped red line indicates the age-based maximum heart rate.

APPENDIX D
VISUALIZATIONS: FATIGUE METRICS

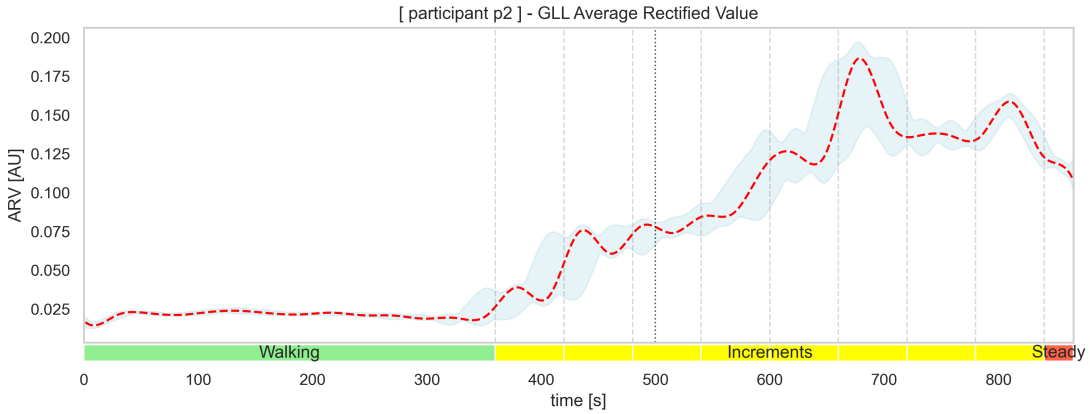

(a) ARV for GLL

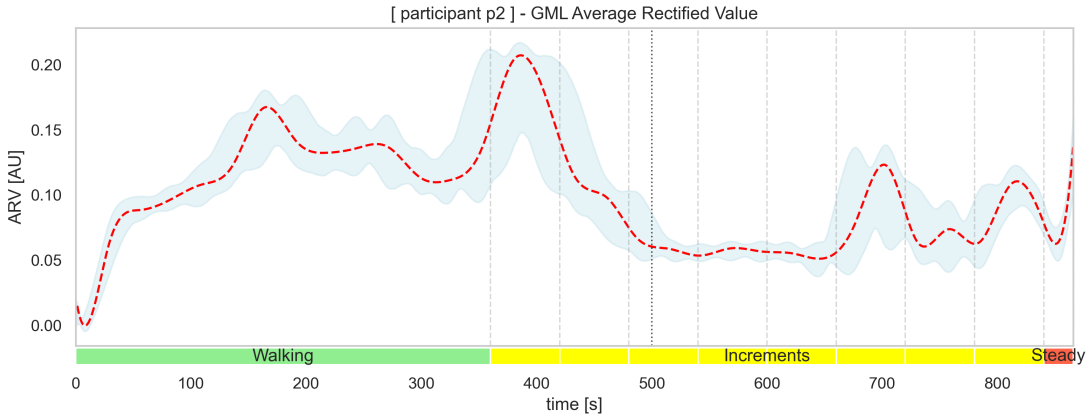

(b) ARV for GML

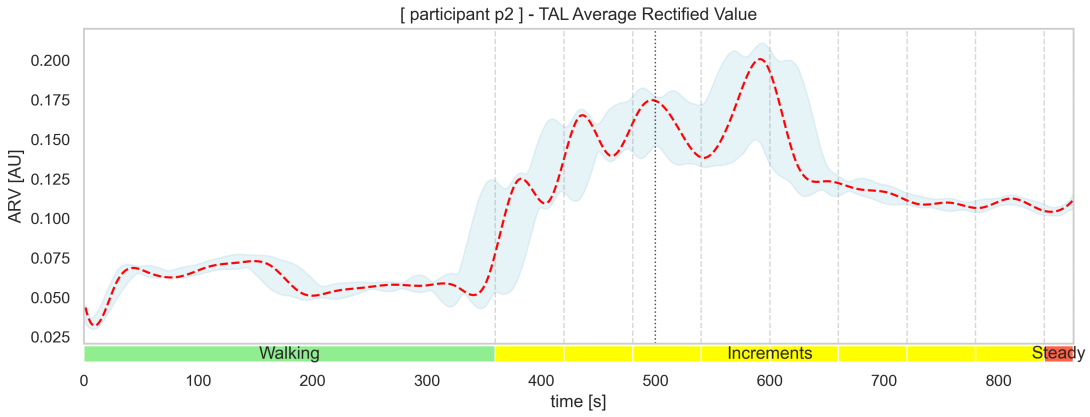

(c) ARV for TAL

Fig. 11: ARV metrics for participant 2 across different muscles.

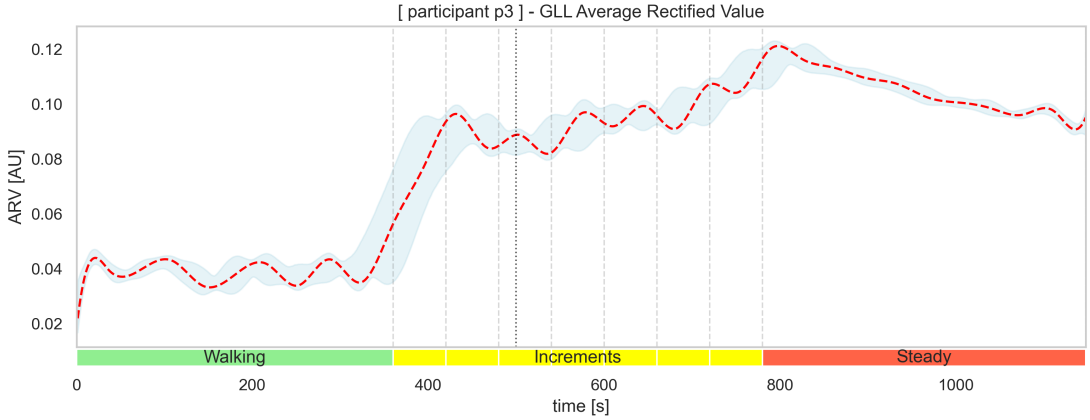

(a) ARV for GLL

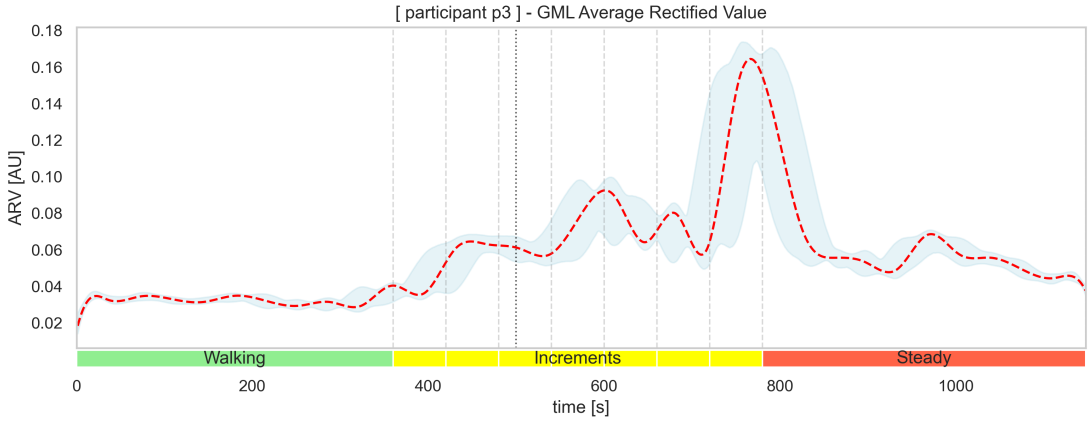

(b) ARV for GML

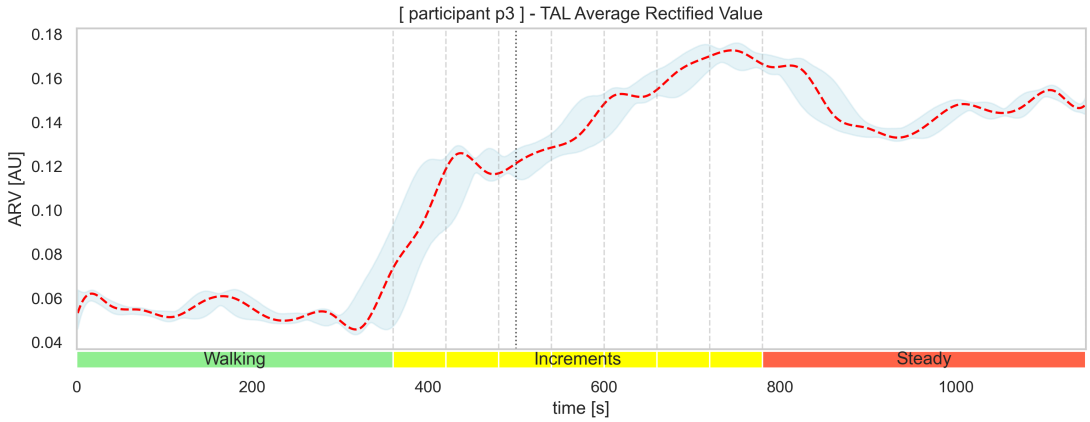

(c) ARV for TAL

Fig. 12: ARV metrics for participant 3 across different muscles.

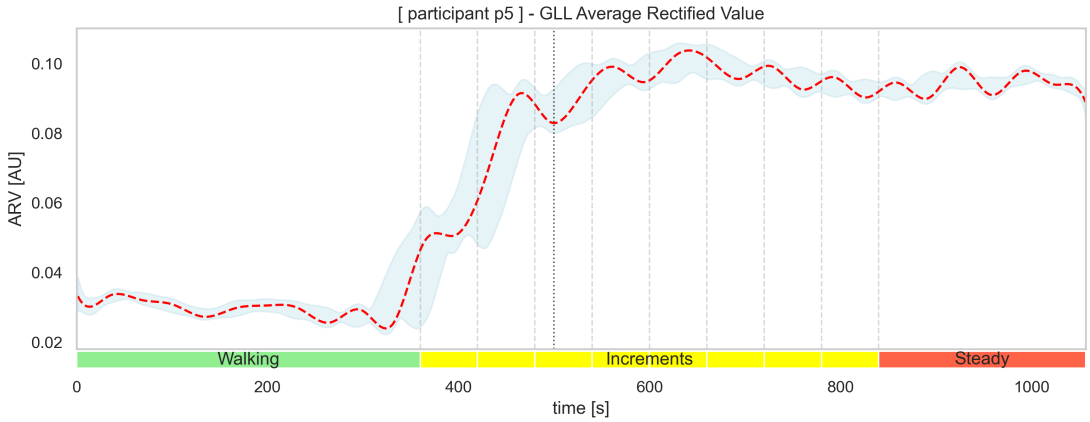

(a) ARV for GLL

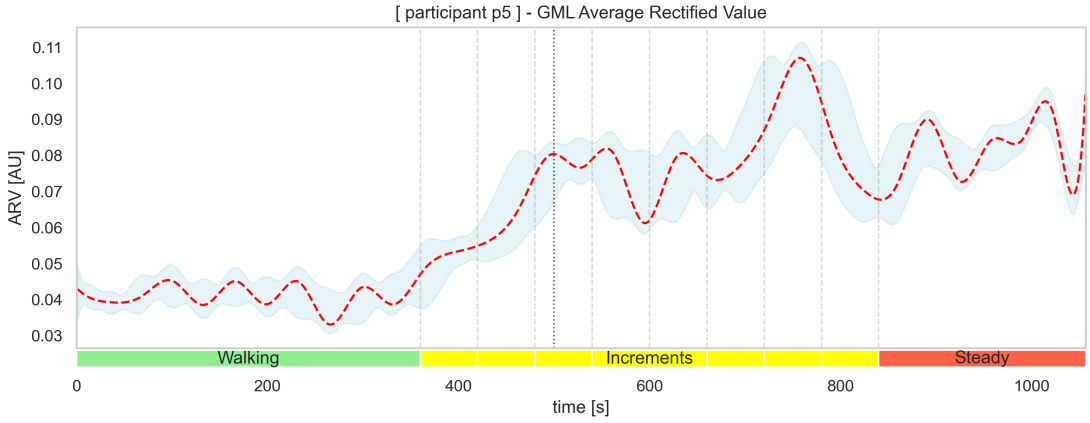

(b) ARV for GML

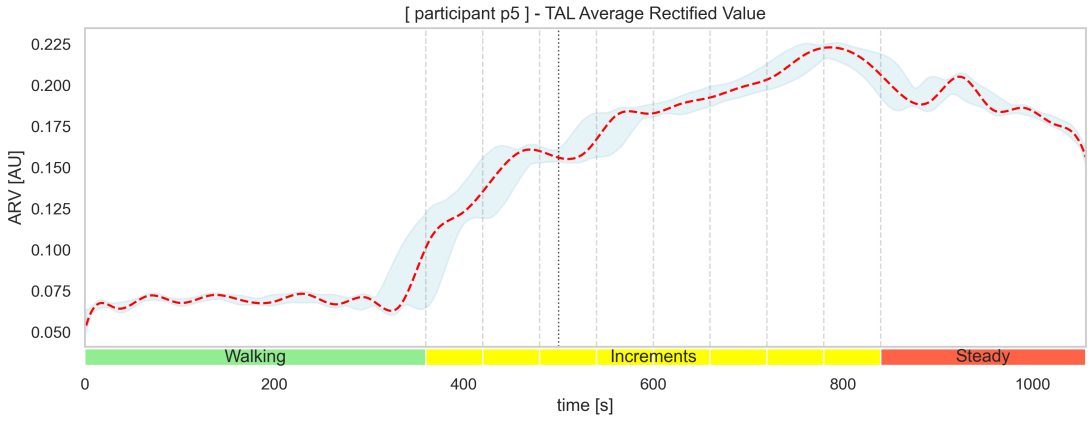

(c) ARV for TAL

Fig. 13: ARV metrics for participant 5 across different muscles.

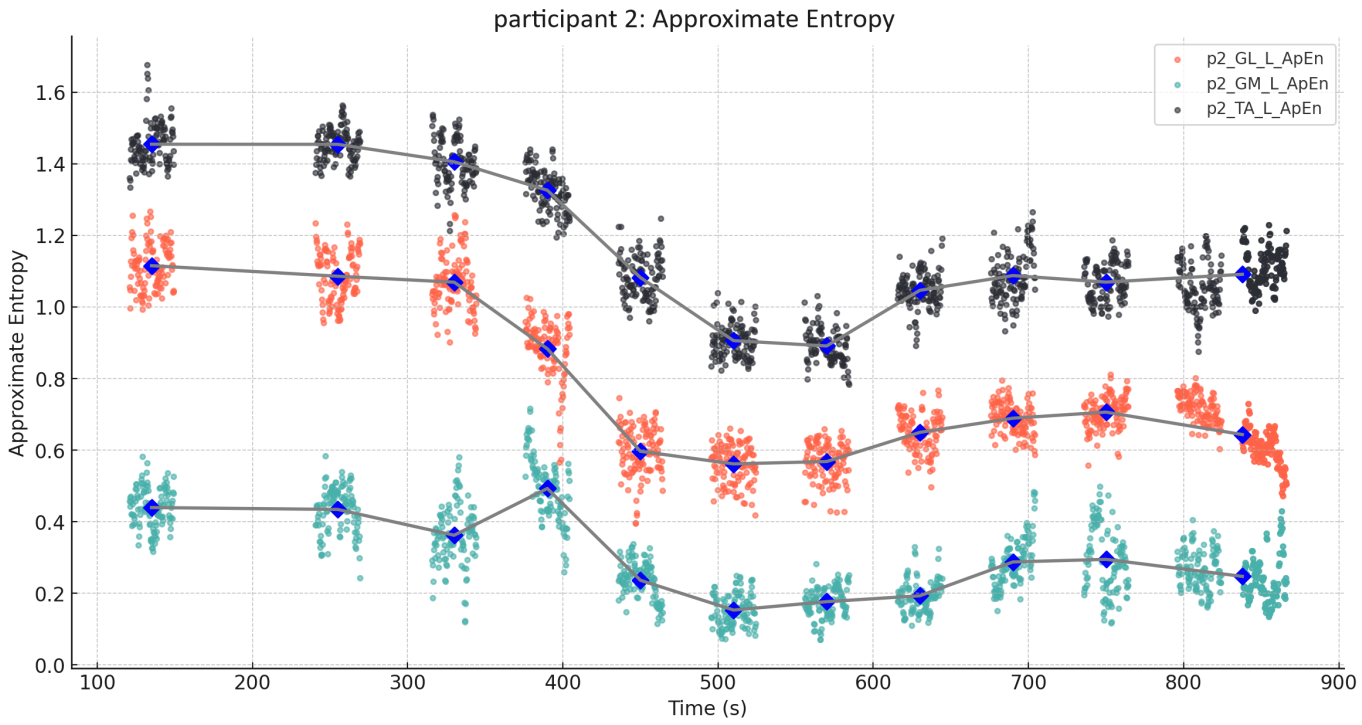

Fig. 14: Approximate Entropy (ApEn) values for the gastrocnemius (GL_L and GM_L), and tibialis anterior (TA_L) muscles for participant 2. Blue markers indicate the cluster mean value for each muscle group

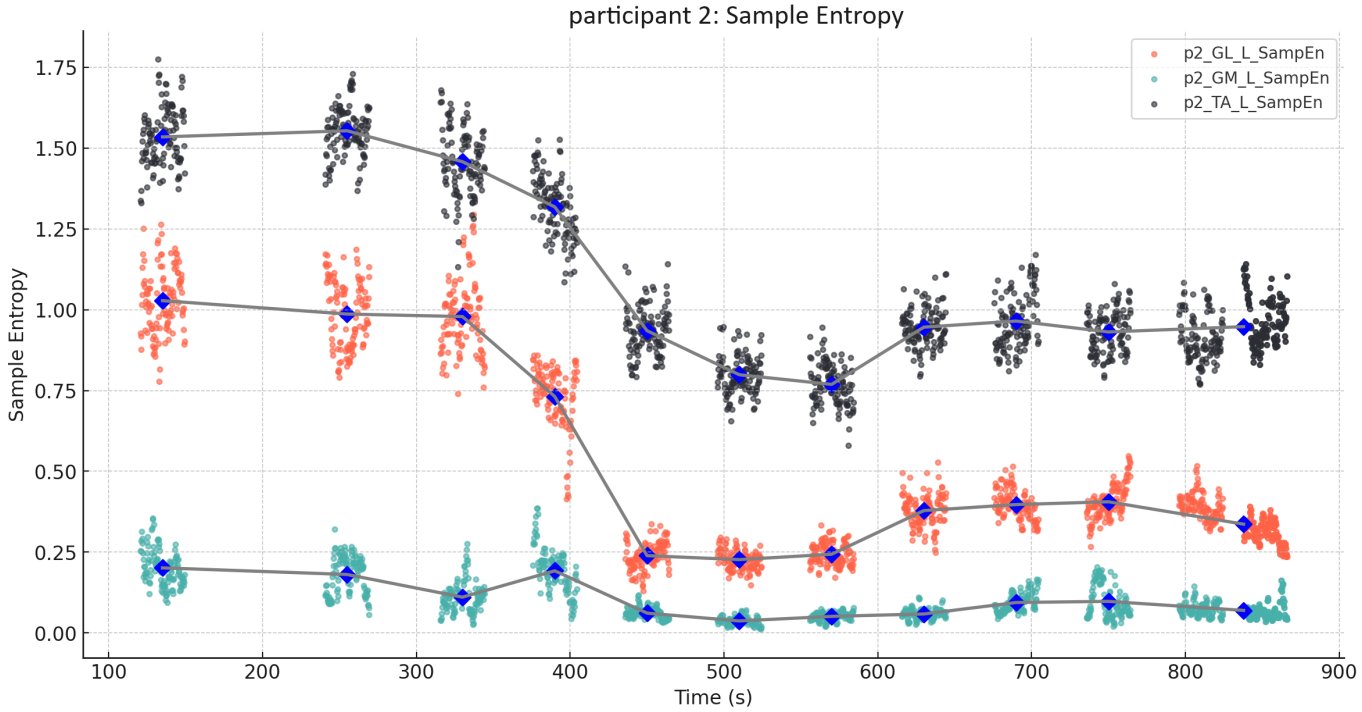

Fig. 15: Sample Entropy (SampEn) values for the gastrocnemius (GL_L and GM_L), and tibialis anterior (TA_L) muscles for participant 2. Blue markers indicate the cluster mean value for each muscle group

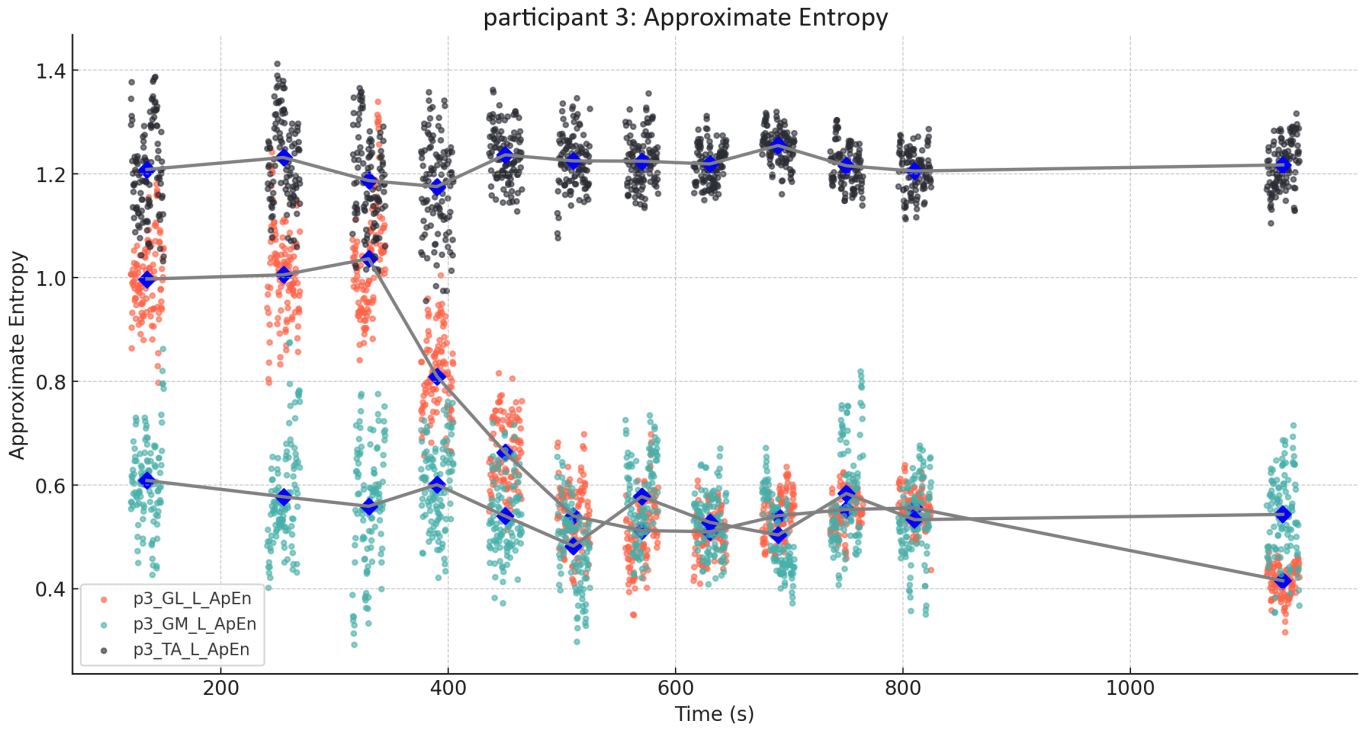

Fig. 16: Approximate Entropy (ApEn) values for the gastrocnemius (GL_L and GM_L), and tibialis anterior (TA_L) muscles for participant 3. Blue markers indicate the cluster mean value for each muscle group

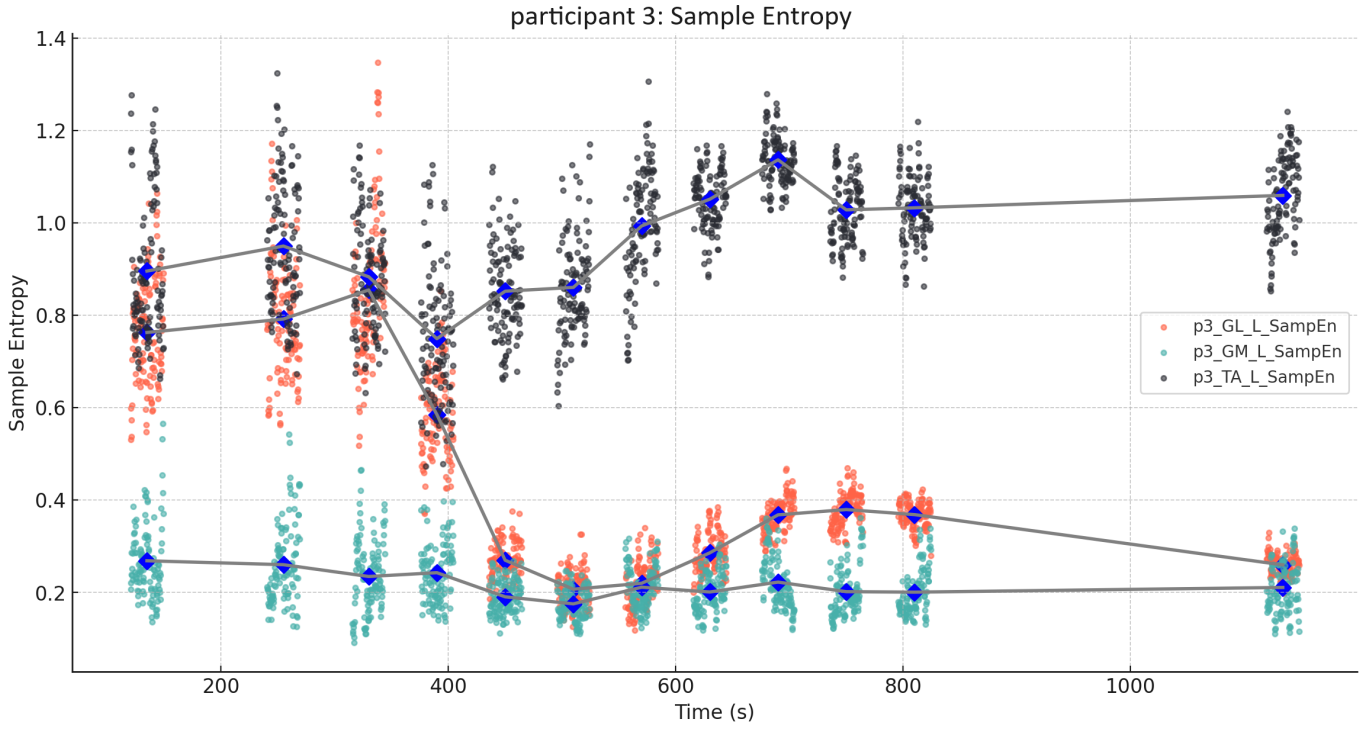

Fig. 17: Sample Entropy (SampEn) values for the gastrocnemius (GL_L and GM_L), and tibialis anterior (TA_L) muscles for participant 3. Blue markers indicate the cluster mean value for each muscle group

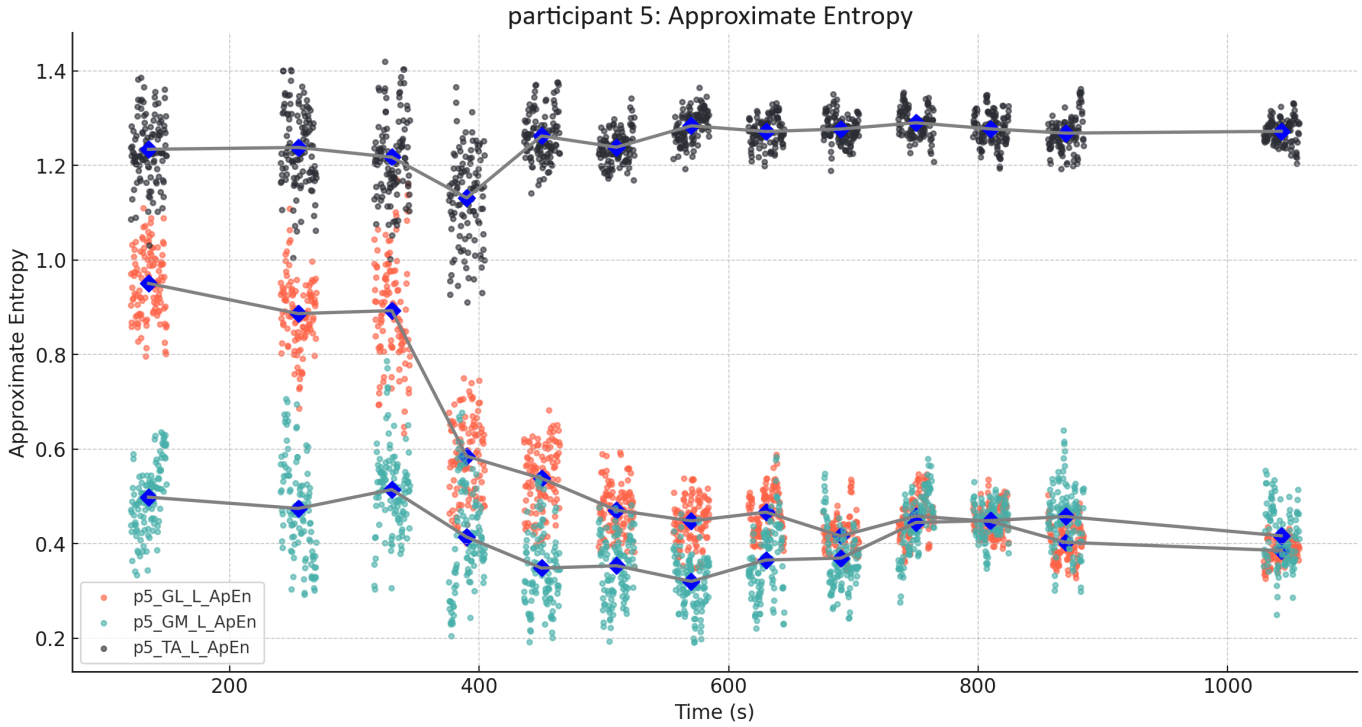

Fig. 18: Approximate Entropy (ApEn) values for the gastrocnemius (GL_L and GM_L), and tibialis anterior (TA_L) muscles for participant 5. Blue markers indicate the cluster mean value for each muscle group

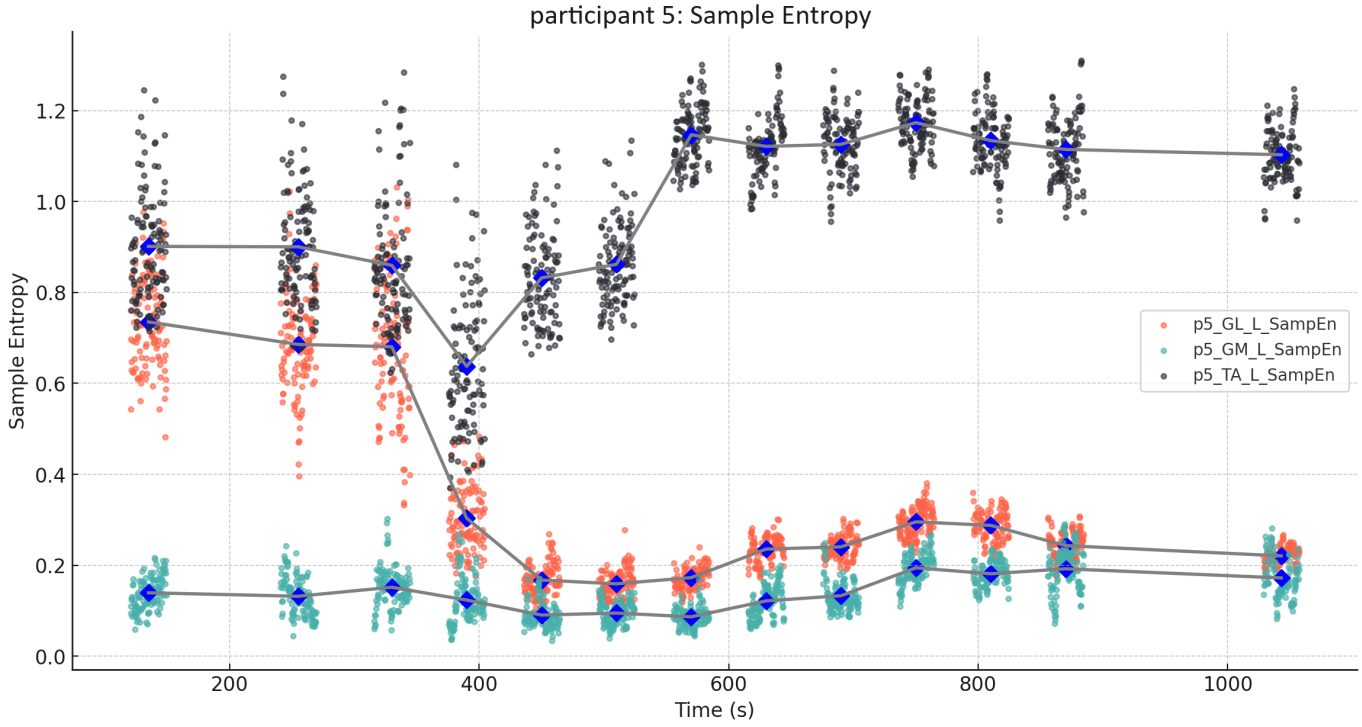

Fig. 19: Sample Entropy (SampEn) values for the gastrocnemius (GL_L and GM_L), and tibialis anterior (TA_L) muscles for participant 5. Blue markers indicate the cluster mean value for each muscle group

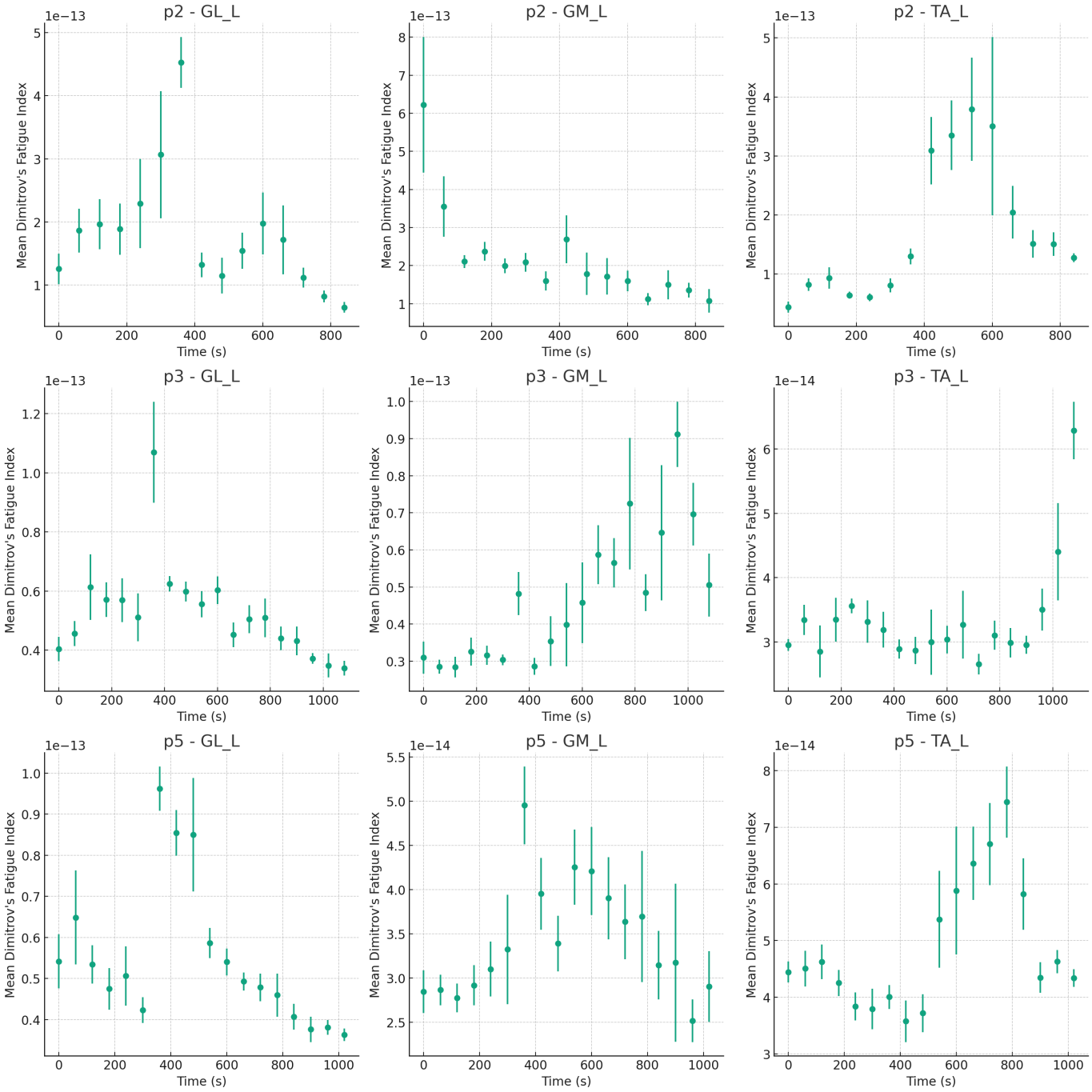

Fig. 20: Dimitrov's Spectral Fatigue Index (FInsm5) for participant 2, 3 and 5. Dots represents binned means with MAD as error bars.

APPENDIX E
SUPPLEMENTARY DATA

Borg's Scale of Perceived Exertion (RPE)	
Rating	**Interpretation**
6	-
7	very, very light
8	-
9	very light
10	-
11	fairly light
12	-
13	somewhat hard
14	-
15	hard
16	-
17	very hard
18	-
19	very, very hard
20	-

TABLE XI: Borg's Rating of Perceived Exertion (RPE) Scale. Comprehensive overview of Borg's RPE scale, detailing each rating number alongside its corresponding interpretation. It serves as a guide for understanding the subjective levels of exertion experienced by participants, ranging from minimal effort to maximal exertion.

Participant	Gender	Height	Weight	Age
p1	m	188	86	25
p2	m	180	97	27
p3	m	188	84	28
p4	m	180	64	25
p5	m	190	86	27

TABLE XII: participant information. Gender male (m), height in [cm], weight in [kg], age in [years]